AD-A110 506 SRI INTERNATIONAL MENLO PARK CA F/G 11/6
NONLINEAR ELECTROMAGNETIC SCATTERING TECHNIQUES FOR THE DETECTI--ETC(U)
NOV 81 A J BAHR, J P WATJEN, J H GIOVANOLA F44620-79-C-0005
UNCLASSIFIED AFOSR-TR-82-0017 NL

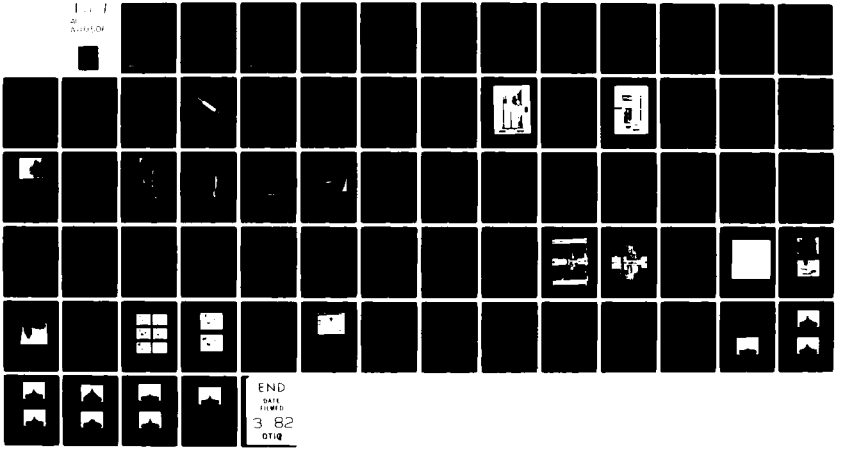

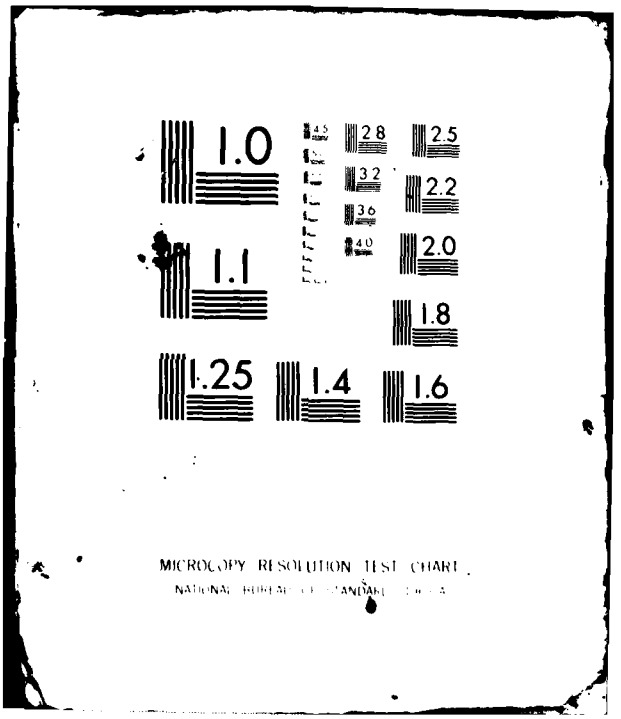
1.0
1.1
1.25
1.4
1.6
1.8
2.0
2.2
2.5
2.8
3.2
3.6
4.0
MICROCOPY RESOLUTION TEST CHART

LEVEL II

12

Final Report
Covering the Period 1 October 1980 to 30 September 1981

November 1981

NONLINEAR ELECTROMAGNETIC SCATTERING TECHNIQUES FOR THE DETECTION AND CHARACTERIZATION OF CLOSED CRACKS

By: A. J. BAHR J. P. WATJEN J. H. GIOVANOLA

Prepared for:

AIR FORCE OFFICE OF SCIENTIFIC RESEARCH
DIRECTORATE OF ELECTRONIC AND
SOLID STATE SCIENCES
BOLLING AIR FORCE BASE, BUILDING 410
WASHINGTON, D.C. 20332

Attention: CAPT. STEVEN G. WAX
Program Manager, AFOSR/NE

CONTRACT F44620-79-C-0005

SRI Project 7908

Approved for Public Release: Distribution Unlimited.

SRI International
333 Ravenswood Avenue
Menlo Park, California 94025
(415) 326-6200
Cable: SRI INTL MPK
TWX: 910-373-1246

SRI International

Final Report
Covering the Period 1 October 1980 to 30 September 1981

November 1981

NONLINEAR ELECTROMAGNETIC SCATTERING TECHNIQUES FOR THE DETECTION AND CHARACTERIZATION OF CLOSED CRACKS

By: A. J. BAHR J. P. WATJEN J. H. GIOVANOLA

Prepared for:

AIR FORCE OFFICE OF SCIENTIFIC RESEARCH
DIRECTORATE OF ELECTRONIC AND
SOLID STATE SCIENCES
BOLLING AIR FORCE BASE, BUILDING 410
WASHINGTON, D.C. 20332

Attention: CAPT. STEVEN G. WAX
Program Manager, AFOSR/NE

CONTRACT F44620-79-C-0005

SRI Project 7908

Approved for Public Release: Distribution Unlimited.

Approved by:

LAWRENCE E. SWEENEY, *Director*
Remote Measurements Laboratory

DAVID A. JOHNSON, *Vice President*
System Technology Division

SRI INTERNATIONAL, 333 Ravenswood Avenue, Menlo Park, California 94025
(415) 326-6200, Cable: SRI INTL MPK, TWX: 910-373-1246

UNCLASSIFIED

SECURITY CLASSIFICATION OF THIS PAGE (When Data Entered)

REPORT DOCUMENTATION PAGE	READ INSTRUCTIONS BEFORE COMPLETING FORM
1. REPORT NUMBER AFOSR-TR-82-0017 2. GOVT ACCESSION NO. AD-A110506	3. RECIPIENT'S CATALOG NUMBER
4. TITLE (and Subtitle) Nonlinear Electromagnetic Scattering Techniques for the Detection and Characterization of Closed Cracks	5. TYPE OF REPORT & PERIOD COVERED Final Report Covering Period 1 October 1980 to 30 September 1981
	6. PERFORMING ORG. REPORT NUMBER SRI Project 7908
7. AUTHOR(s) A. J. Bahr, J. P. Watjen, and J. H. Giovanola	8. CONTRACT OR GRANT NUMBER(s) Contract F44620-79-C-0005
9. PERFORMING ORGANIZATION NAME AND ADDRESS SRI International Menlo Park, California 94025	10. PROGRAM ELEMENT, PROJECT, TASK AREA & WORK UNIT NUMBERS 61102F 2306/A2
11. CONTROLLING OFFICE NAME AND ADDRESS Air Force Office of Scientific Research (AFOSR/NE) Bldg. 410, Bolling AFB, Washington, D.C. 20332	12. REPORT DATE November 1981 / 13. NO. OF PAGES 74
14. MONITORING AGENCY NAME & ADDRESS (if diff. from Controlling Office)	15. SECURITY CLASS. (of this report) Unclassified
	15a. DECLASSIFICATION/DOWNGRADING SCHEDULE

16. DISTRIBUTION STATEMENT (of this report)

Approved for Public Release; Distribution Unlimited

17. DISTRIBUTION STATEMENT (of the abstract entered in Block 20, if different from report)

18. SUPPLEMENTARY NOTES

19. KEY WORDS (Continue on reverse side if necessary and identify by block number)

Surface-Crack Detection
Nondestructive Evaluation
Nonlinear Scattering
Eddy Currents
Metal-Oxide-Metal Junctions
Fatigue-Crack Growth

20. ABSTRACT (Continue on reverse side if necessary and identify by block number)

The research described in this report seeks to develop an improved nondestructive evaluation (~~NDE~~) technique for detecting and characterizing tightly closed cracks on surfaces of metal parts. This new technique is based on exploiting the nonlinear eddy-current interaction that would occur if a nonlinear junction existed between the faces of a closed crack. Both second- and third-harmonic signals in the 1- to 3-GHz range have been detected emanating from cracks in flat samples of aluminum and copper. The third-harmonic signals were typically four orders of magnitude larger than the second-harmonic signals. These results suggest that the

DD FORM 1 JAN 73 1473

EDITION OF 1 NOV 65 IS OBSOLETE

UNCLASSIFIED

SECURITY CLASSIFICATION OF THIS PAGE (When Data Entered)

19. KEY WORDS (Continued)

20 ABSTRACT (Continued)

dominant physical mechanism involved is electron tunneling in a metal-oxide-metal junction.

This crack detection technique is not as reliable as desired because it is difficult to keep spurious background levels from masking the desired crack signals, and because nonlinear junctions required for detection do not always form in the crack. However, experiments conducted using modified aluminum compact-tension specimens suggest that monitoring of nonlinear crack signals can yield information on the rate of crack growth.

A simple model for a nonlinear crack also is described. This model shows that the nonlinear signal produced by a crack is strongly dependent on the impedances of the crack at the measurement frequencies, and particularly on the area and thickness of the nonlinear junction. Calculations using this model indicate that the use of frequencies in the low microwave range should produce the largest nonlinear signals. However, quantitative agreement between these calculations and the experimental results is not very good, and so a better model (probably stochastic) is needed.

CONTENTS

ILLUSTRATIONS

ILLUSTRATIONS (Concluded)

ACKNOWLEDGMENTS

The authors wish to thank J. H. Hunt for constructing the microwave probes, N. S. Stafford and R. Elbrecht for help with mechanical design, and D. J. Petro for photographing the metallurgical specimens. In addition, A. Rosengreen, L. J. Kaplan, and M. M. Vargas all made valuable contributions to the modeling of a nonlinear crack. Discussions during th. earlier phases of this program with R. Jones, B. Syrett, and L. E. Eiselstein on questions relating to materials and materials testing also were very valuable. Finally, the information provided by B. A. Auld of Stanford University on his theory of the linear interaction of eddy currents with cracks in metals played a key role in the development of the nonlinear crack model, and was very much appreciated.

I INTRODUCTION

The research being carried out under this program is aimed at meeting the Air Force requirement for improved nondestructive evaluation (NDE) techniques to reduce the operating and support costs required to maintain a fleet of existing aircraft. The primary objective of SRI's research is to develop a technique for reliably detecting small, tightly closed surface cracks, such as those that occur in the rotating parts of high-performance jet engines.

The technique under study in this research--electromagnetic scattering from nonlinear metal-to-metal junctions--apparently has not been used previously for crack detection. Possible physical mechanisms that could produce a nonlinearity in such junctions are point-contact phenomena and tunneling through an intervening oxide layer. In this technique, the nonlinear junction is illuminated by electromagnetic energy at one or more frequencies, and either a harmonic of the fundamental frequency or an intermodulation-product frequency is detected. The sensitivity of this technique in detecting small closed cracks is potentially very high because the detected signal can be filtered so that it can be discriminated from clutter generated by linear scattering mechanisms.

Electromagnetic scattering from a nonlinear junction is a well-known phenomenon that has both caused problems and been useful, depending on the situation. For example, interfering frequencies are often generated by nonlinear junctions situated in the neighborhood of radar or communication transmitting antennas on ships,[1,2*] or even within the antenna structure itself.[3,4] On the other hand, this effect already has been used in applications requiring the locating of metallic objects hidden in vegetation.[5]

---

*References are listed at the end of the report.

One objective of the research described in this report is to extend this latter technique one step further--i.e., to locate the nonlinear junction itself on the surface of the metallic object; the assumption being that detection of a nonlinear junction in an otherwise homogeneous metallic surface is indicative of a closed crack. This nonlinear testing technique has been used successfully to determine the presence of flaws in passive electronic components,[6,7] in which case the test equipment was connected directly to the components for the purpose of applying and detecting the desired signals. In the crack-detection situation, however, the signals are applied and detected by means of an inductively or capacitively coupled probe.

Another objective of this research is to evaluate the sensitivity, background discrimination, and other parameters associated with the nonlinear crack-detection technique.

A final objective is to determine the ability of the technique to characterize the dimensions of closed surface cracks, or any other physical parameters that are important in determining the likelihood that a crack will propagate unstably and cause catastrophic component failure under service conditions.

This report describes the results obtained during the third year of this research program. In summary, we have shown that third-order nonlinear contacts can exist in fatigue cracks in a material such as aluminum, and that harmonic or intermodulation signals generated by such contacts can be detected in the 1- to 3-GHz frequency range. However, it appears that the presence of such contacts in a crack depends on the loading history of the part containing the crack. Thus, seeking to detect signals generated by a nonlinear contact does not represent a reliable crack-detection method. However, this method may be applied to monitoring the rate of crack growth.

To date, this research has resulted in the publishing of the following papers:

(1) A. J. Bahr, "Microwave Detection of Third-Order Nonlinearities in Fatigue Cracks," Electronics Letters, Vol. 16, pp. 150-152 (February 1980).

(2) A. J. Bahr, "Theory of Scattering from a Nonlinearly Loaded Aperture," IEEE Trans. Antennas Propagat., Vol. AP-28, pp. 840-845 (November 1980).

II SUMMARY OF PREVIOUS RESULTS

Before presenting the results of our third year of research, it is useful to place them in context by briefly reviewing the results obtained during the first two years of this program.

Much of the effort on this program has been directed at demonstrating the existence of the postulated electromagnetic nonlinearity in a surface-breaking fatigue crack. This goal was finally achieved during the third year after we tried several different measurement systems, frequencies, electromagnetic probes, materials, and types of samples.

The choice of a measurement system for detecting an electromagnetic nonlinearity in a crack involves the consideration of a number of factors, including operating frequency range, number of frequencies applied, ability to realize optimum transmitting and receiving probes, and ability to reject spurious background signals.

In discussing these factors, it is useful first to list the frequencies that are generated by a particular order of nonlinearity. In practice, it is sufficient to consider only second- or third-order nonlinearities since higher-order nonlinearities can be expected to be relatively small. A second-order nonlinearity is one in which the input variable is proportional to the square of the output variable. For example, the current flowing in a second-order nonlinear conductance is proportional to the square of the voltage across that conductance. Similarly, for a third-order nonlinearity, the input variable is proportional to the cube of the output variable. Thus, if the excitation is considered to be composed of two monochromatic signals with noncommensurate frequencies, f_1 and f_2, it is found that a second-order nonlinearity produces frequencies at 0, $2f_1$, $2f_2$, $f_1 - f_2$, and $f_2 + f_2$. Similarly, a third-order nonlinearity produces the frequencies f_1, f_2, $3f_1$, $3f_2$, $2f_1 + f_2$, $2f_1 - f_2$, $2f_2 + f_1$, and $2f_2 - f_1$. These spectra are illustrated in Figure 1. It can be seen that the spectra

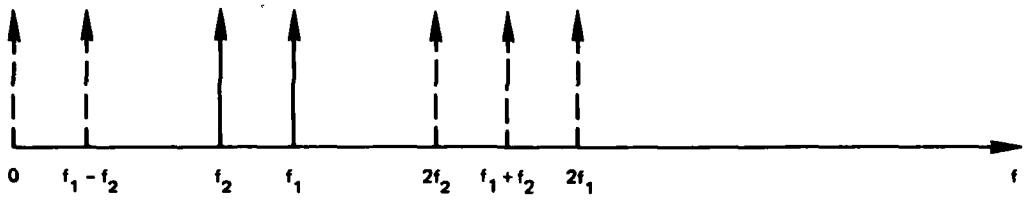

(a) SECOND – ORDER NONLINEARITY

(b) THIRD – ORDER NONLINEARITY

FIGURE 1 SPECTRA FOR TWO-FREQUENCY EXCITATION OF A NONLINEAR JUNCTION

corresponding to the second- and third-order nonlinearities do not overlap, and so, in principle, the relative strengths of these nonlinearities can be compared by detecting the corresponding frequencies.

The simplest spectrum is obtained by using single-frequency excitation. For this case, Figure 1 shows that the frequencies generated by the nonlinearity will all be harmonically related to the applied frequency, which means that they will be higher than the applied frequency. This situation may necessitate the use of separate transmitting and receiving probes if the bandwidth of a single probe is not large enough. However, a problem with using two separate probes is that it is likely that the two probes will physically interfere with one another. In addition, if the applied frequency is in the high microwave region, the receiver for the harmonic frequencies becomes difficult and expensive to realize.

Figure 1 shows that, when two frequencies are applied, the nonlinearly generated frequencies lie in the vicinity of both the harmonic frequencies and the low frequencies for a second-order nonlinearity, and near both the harmonic frequencies and the applied frequencies for a third-order nonlinearity. Thus, for two-frequency excitation one has the option of detecting frequencies that are quite different from the harmonic frequencies, namely, the difference frequency, $f_1 - f_2$, for a second-order nonlinearity, or an intermodulation frequency, say $2f_2 - f_1$, for a third-order nonlinearity.

Thus, our first attempt to detect an electromagnetic nonlinearity in a crack used a two-frequency system, which is described in detail in Reference 8. An operating frequency near 10 GHz was chosen in the belief that this choice would result in a high sensitivity.* Since it has been reported that the third-order nonlinearity is strongest in junctions between metal parts,[1,6] the system was configured to detect the third-order intermodulation frequency $2f_2 - f_1$.

For this system, initial consideration was given to the use of radiating probes such as horns, open-ended waveguides, and the like, since they offer the advantage of not requiring physical contact with the surface being inspected. However, such radiating probes are disadvantageous because they permit the high-level interrogating signals to interact with nearby nonlinearities or to leak more easily into the receiver. In addition, they do not concentrate the eddy currents as well as a near-field probe; therefore, a small coaxial near-field probe was developed for use with the microwave system.

This coaxial microwave probe consisted of a half-wavelength-long dipole printed on a thin dielectric sheet. The dipole was connected to a coaxial line (either semirigid or flexible) through a balun. The balun consisted of a pair of quarter-wavelength-long slots cut diametrically

*Later analysis showed that, in fact, the sensitivity should be higher at somewhat lower frequencies.

opposite to one another in the outer conductor of the coaxial line and backed by several ferrite beads. When the dipole is placed against a metal surface, its radiation becomes negligible and it becomes a resonant section of microstrip transmission line. This type of probe concentrates the eddy currents in a region near the center of the dipole. Figure 2 is a photograph of the assembled probe.

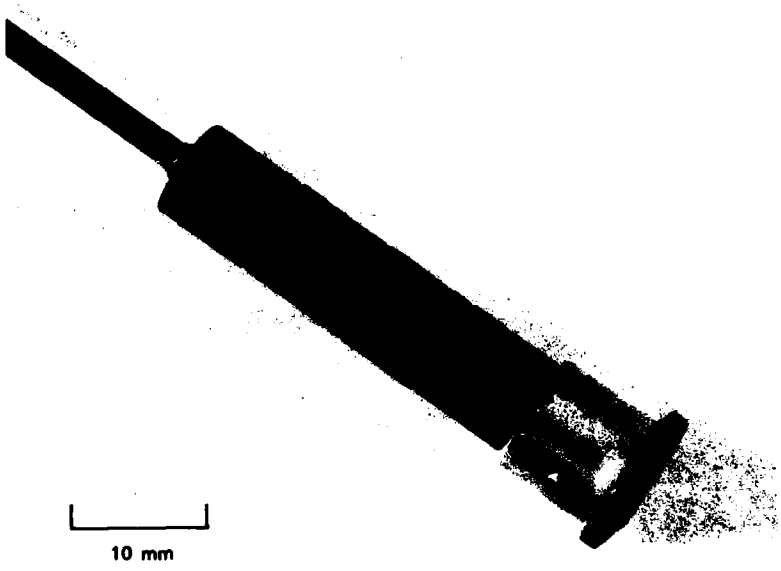

FIGURE 2 MICROSTRIP EDDY-CURRENT PROBE

Several notched specimens (similar to compact-tension specimens) of 6061-T6 aluminum alloy and type 304 stainless steel were prepared. Fatigue cracks initiating at the notch and extending throughout the thickness of the specimen were grown using cyclic loading. By placing the microwave probe on the side of the specimen near the mouth of each crack, we observed that third-order signals were generated by both types of material. This demonstrated for the first time (to the best of our knowledge) that third-order nonlinearities can exist in this type of crack.

With +33 dBm applied at each frequency, the power in the third-order signals was on the order of -105 dBm, and the signal-to-noise ratio (SNR) was in excess of 20 dB.

Next, to test the hypothesis that the two contacting metal surfaces must be separated by an oxide for the third-order nonlinearity to be observed, we carried out some simple experiments with the microwave system. The idea behind these experiments was to form metal-to-metal contacts both with and without intervening oxides, and then to compare the third-order signals produced by these contacts. We knew of no way to form such specific contacts using real cracks, so we simply created the junctions by touching two pieces of metal together. To obtain the small contact areas required for the nonlinear effect to be observed at microwave frequencies, we bent thin strips of metal so that contact always was made along a sharp edge of one of the two pieces forming the test junction.

Pure gold does not directly form an oxide. Therefore, we used pure gold (0.9999) as one side of the junction and touched it with strips of aluminum, copper, and gold. According to our hypothesis, aluminum and copper should have produced strong third-order signals, while gold should not have produced any nonlinear signal.

As expected, the aluminum-gold and copper-gold junctions produced large signals, while the gold-gold junction did not produce any detectable signal. A substantial effort was made to obtain a signal from this junction by adjusting the contact, but none was obtained. On the other hand, it was easy to obtain repeatable results with the aluminum-gold and copper-gold contacts.

Although these findings do not prove that it is necessary for an oxide to exist in a crack for a nonlinear signal to be observed, they certainly suggest that this is the case for nonmagnetic metals.

Next, we attempted to use the microwave system to detect third-order nonlinearities in tight surface-breaking fatigue cracks in aluminum plates. Even though these cracks were several millimeters long, we were unsuccessful. We reasoned that the cracks were being short-circuited by

displacement currents at our operating frequency of 10 GHz, and so we concluded that we should repeat the tests at lower frequencies.

Without a model to suggest how low in frequency we should go, we selected a frequency of 100 kHz, where we knew that conventional eddy current crack-detection systems were quite sensitive. We attempted to detect third-order nonlinearities in both real and simulated cracks in metal plates and bars using two-frequency excitation of three different kinds of probes, but we were unsuccessful in all cases.

About this time we became aware of the work of Auld[9] in modeling the interaction between an electromagnetic probe and a surface-breaking crack. By combining his model with the Volterra-series analysis of weakly nonlinear circuits described by Bussgang et al,[10] we were able to develop an approximate model for a crack containing a nonlinear contact uniformly located across the crack mouth.* The results of calculations using this model suggested that greater sensitivity might be obtainable by operating in the 1- to 3-GHz frequency range.

The results of third-year program experiments aimed at detecting second- and third-harmonic signals in the 1- to 3-GHz range produced by cracks in flat samples are presented in Section III, which also describes the microwave probes used for these experiments. Section IV describes a circuit model for a nonlinear crack and presents the results of a sample calculation for the third-harmonic probe. The interesting results obtained by detecting the third-harmonic signals emanating from a growing crack in a modified aluminum compact-tension specimen undergoing cyclic loading are presented and discussed in Section V. Finally, the conclusions derived from this research are given in Section VI. The actual experimental data for the third-harmonic responses of cracks in flat samples are contained in the Appendix.

*A detailed discussion of this model is presented in Section IV.

III EXPERIMENTAL RESULTS FOR CRACKS IN FLAT SAMPLES

A. General

To test the possibility of achieving greater sensitivity to the nonlinear signals generated by tight cracks by operating at a frequency between 1 and 3 GHz, we carried out some experiments in this range using real and simulated cracks in flat samples. Rather than use two-frequency excitation, it proved to be simpler to use single-frequency (1-GHz) excitation. We constructed two special near-field probes for these tests: one was designed to detect the second harmonic at 2 GHz, and the other was designed to detect the third harmonic at 3 GHz. The materials tested were soft iron, stainless steel, aluminum, and copper. However, the iron and steel generated such large nonlinear responses due to their nonlinear permeability that the flaw signals could not be discerned. Consequently, the major portion of the experimental evaluation was limited to testing of aluminum and copper samples.

The following sections will describe the probes, the samples, and the experimental results. The actual experimental data are presented in the Appendix.

B. Probes

Both the second- and third-harmonic probes developed for this program were based on a quarter-wave, microstrip-resonator eddy-current probe that was developed by SRI for the U.S. Air Force under separate contract.[11] This type of probe, shown in Figure 3, consists of a length of microstrip transmission line one-quarter wavelength long and short circuited at one end. The end of the resonator opposite the short-circuit is capacitively coupled to the exciting and receiving portion of the system. In practice, the short-circuited end of the resonator is pressed against the sample being tested. To insulate the probe from the sample, Scotch 810

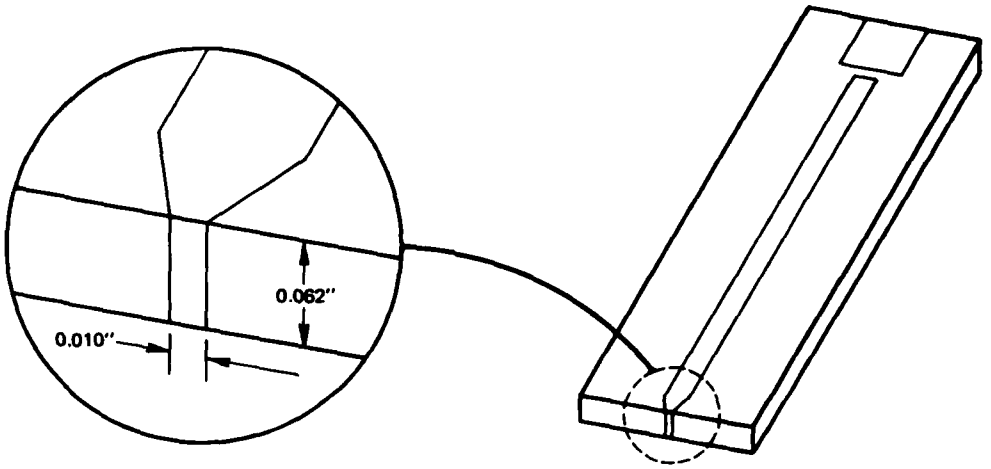

FIGURE 3 SCHEMATIC ILLUSTRATION OF MICROSTRIP-RESONATOR PROBE

tape (0.002-in. thick) was used. This type of probe design maximizes the magnetic field in the probe/flaw interaction region, and has been found to be quite sensitive as an eddy-current probe.

In the third-harmonic probe, tuning elements were added to the basic quarter-wave resonator so that the resonator could be made resonant at both the fundamental and third-harmonic frequencies. The resonator is coupled to an impedance-matching diplexer that simultaneously matches the probe impedance to the source impedance at 1 GHz, and separates the third-harmonic output signal at 3 GHz from the incident signal. A photograph of this probe with its cover removed is shown in Figure 4.

The open-circuited twisted pair that can be seen soldered between ground and the input line in Figure 4 acts as a capacitive tuning element to provide part of the impedance matching. This element was originally a variable capacitor (Johanson p/n 7273), but was changed to the twisted pair when the capacitor was found to generate excessive third-harmonic power. The spurious third-harmonic power generation in this probe was reduced further by soldering the substrate to the enclosure and gold plating the entire assembly. The quarter-wave resonator is enclosed in a channel (top of Figure 4) which is sufficiently narrow to suppress any radiation from this part of the circuit. The microstrip substrate

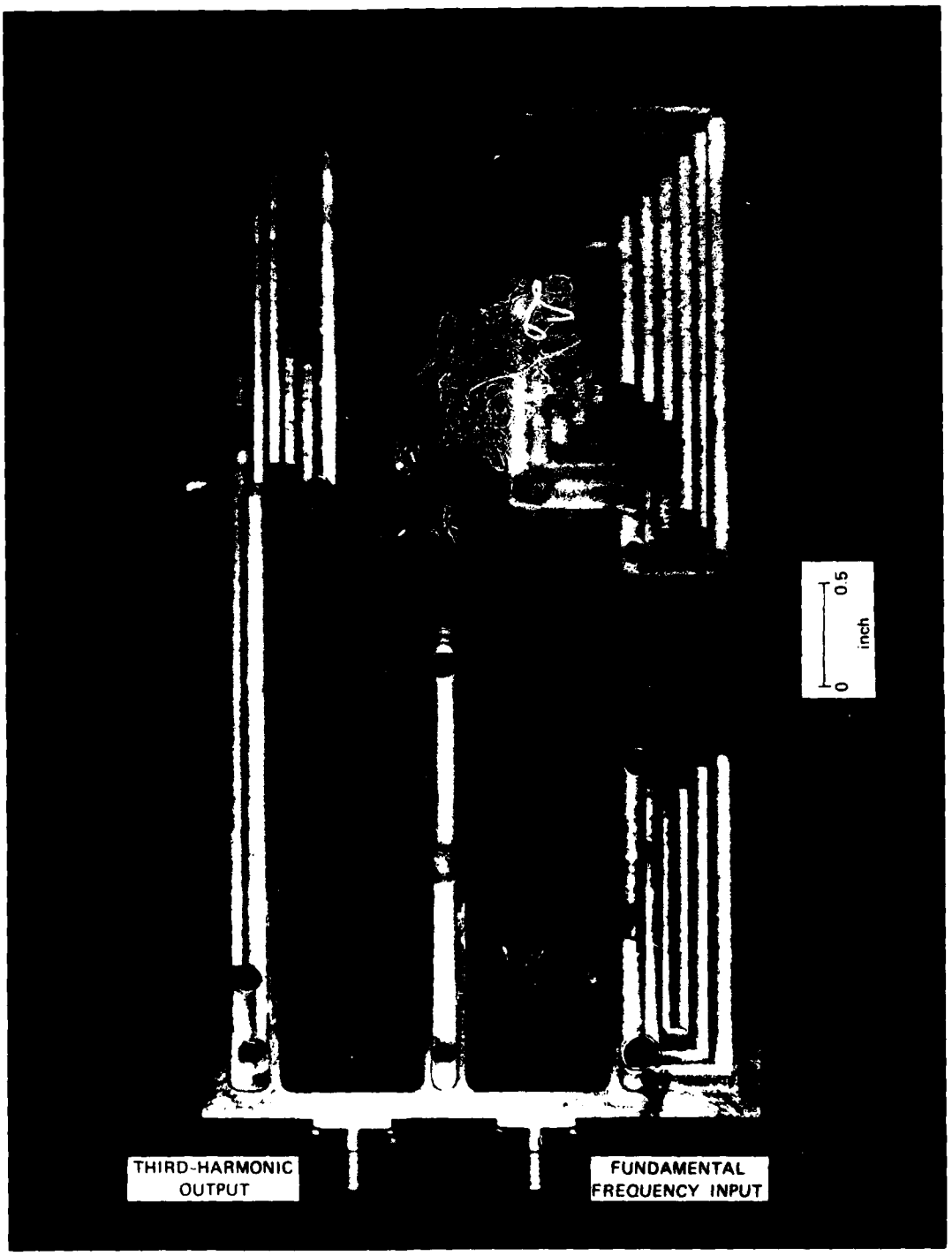

FIGURE 4 THIRD-HARMONIC PROBE WITH COVER REMOVED

is recessed below the enclosure cover approximately 0.5 in. to minimize the current that flows across the enclosure/cover interface. The residual spurious third-harmonic power measured for this probe design was approximately -106 dBm when the input power at the fundamental frequency was +30dBm.

In the second-harmonic probe, two quarter-wave resonators were used, one being resonant at the fundamental frequency and the other at the second-harmonic frequency. This probe was similar mechanically to the third-harmonic probe in that its substrate also was soldered to the enclosure, was gold plated, and had its cover located in a low-current region. The residual spurious second-harmonic power for this probe was below the system sensitivity of -137 dBm. A photograph of this probe with its cover removed is shown in Figure 5.

A block diagram of the measurement system is shown in Figure 6. The low-noise preamplifier shown in the figure was added to the system to increase the dynamic range of the spectrum analyzer, which was adjusted for maximum practical sensitivity. For example, a relatively fast scan time (5 ms) was used to avoid missing the signal generated by a flaw as the sample was scanned manually past the probe tip. The scan width on the spectrum analyzer was 50 kHz overall, and so a synthesized signal source was used to provide the requisite jitter-free signal.

C. Experimental Results

1. General

Two kinds of flawed metallic samples were used in these tests. One type of sample contained an actual fatigue crack that was produced by cyclic bending of a specimen containing a starter notch in its broader surface. After the fatigue crack had been grown, the starter notch was removed by milling and polishing. The second type of sample was produced by warm rolling a metallic cylinder containing an axial hole. This procedure is called roll bonding. By rolling the sample until the center hole closes, a pseudo-crack is obtained that extends all the way through the sample.

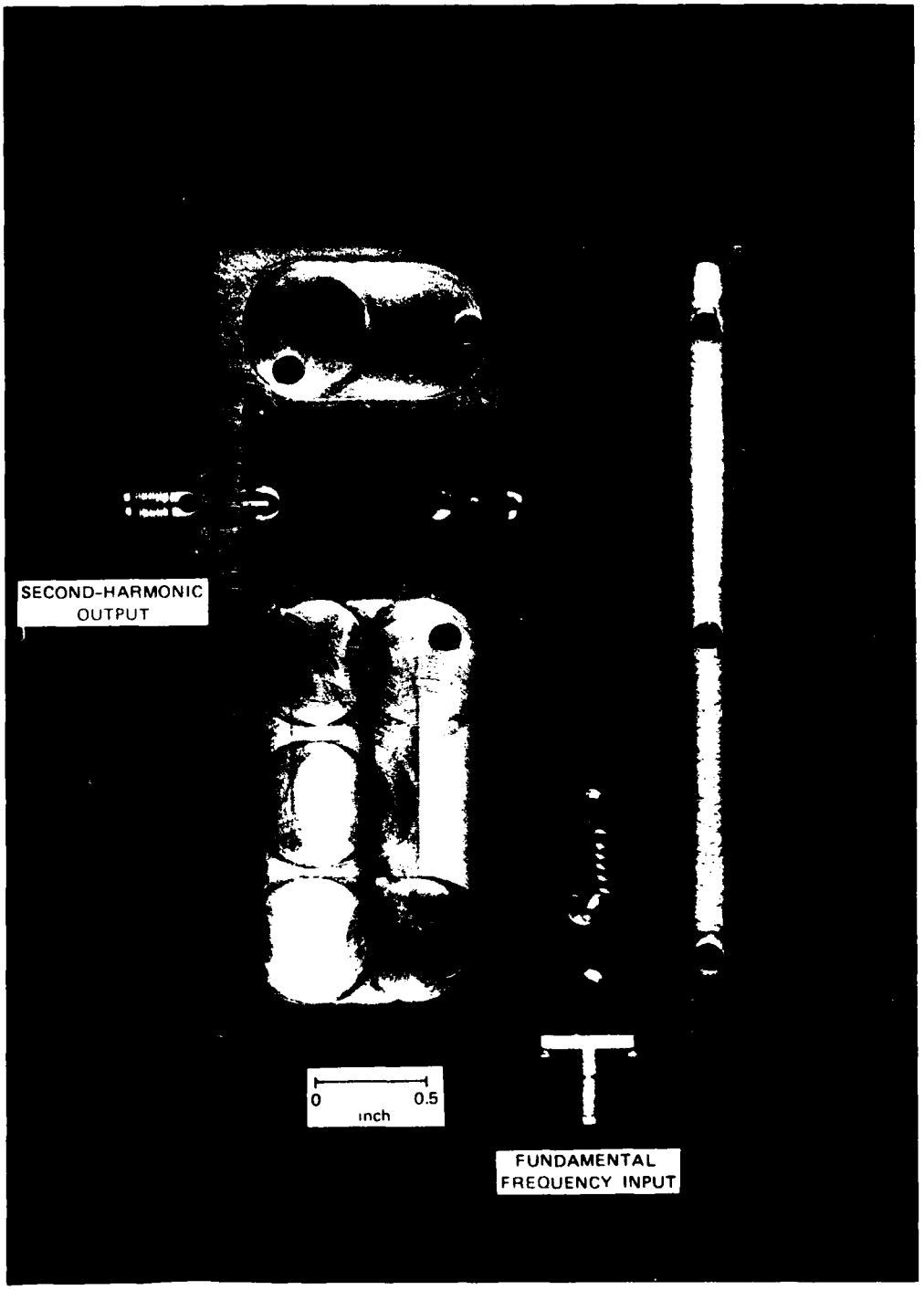

FIGURE 5 SECOND-HARMONIC PROBE WITH COVER REMOVED

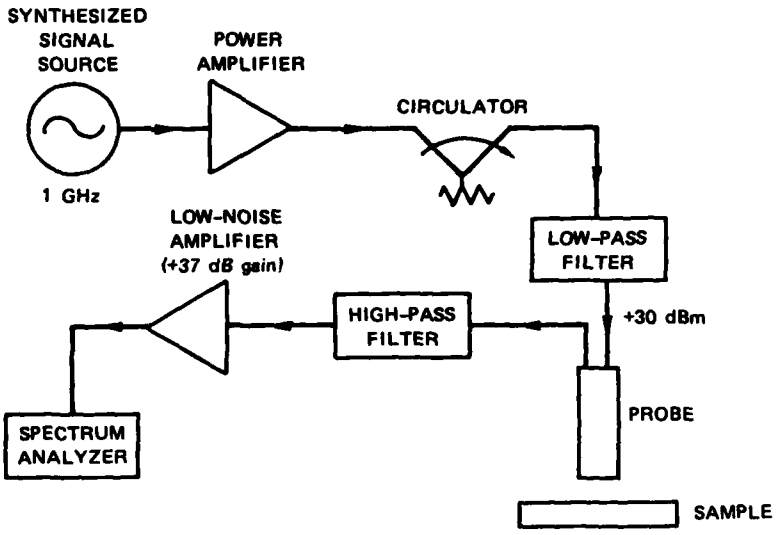

FIGURE 6 BLOCK DIAGRAM OF SYSTEM FOR MEASURING NONLINEAR CRACK SIGNALS

Although great care was taken in the design and fabrication of the probes to minimize internally generated nonlinear signals, such spurious signals nevertheless did occur and were large enough to be the determining factor in establishing the system's flaw-detection sensitivity. The levels of these background signals appeared to be consistent between samples of the same material, but varied somewhat from material to material. The signals were so large in the case of ferrous materials that meaningful flaw data could not be obtained. For reference purposes the background signal level is included in the data for each of the samples.

2. Summary of Results

The following subsections summarize the experimental results. A succinct summary of these results also is given in Table 1. Photographs of the actual nonlinear responses observed on the spectrum analyzer display are presented in the Appendix.

Table 1

SUMMARY OF SECOND- AND THIRD-HARMONIC FLAW RESPONSES

Sample	Second-Harmonic Background (dBm)	Second-Harmonic Flaw Signal (dBm)	Third-Harmonic Background (dBm)	Third-Harmonic Flaw Signal (dBm)
Aluminum B-3	< -137	None	-107	-74
Aluminum C-3	< -137	-125	-107	-82
Aluminum 2	< -137	-127	-107	-74
Aluminum 3	< -137	-125	-107	-82
Aluminum 7	< -137	-125	-107	-49
Aluminum 8	< -137	-125	-107	-100
Copper 9	< -137	-127	-101	-76
Copper 10	< -137	-129	-101	-87

a. Aluminum Samples

Sample B-3

This 2024-T3 aluminum sample contained a single fatigue crack 0.182-in. (4.62-mm) long (see Figure 7). The maximum crack opening was about 2μm. The background signal at the third-harmonic frequency was approximately -107 dBm. The maximum third-harmonic flaw signal was approximately -74 dBm, which was easily detectable. At the second harmonic, the background signal was below the system sensitivity (-137 dBm), but no flaw signal could be detected.

Sample C-3

This sample was also 2024-T3 aluminum and contained a single fatigue crack 0.252 in. (6.40 mm) in length. The crack in this sample was similar in appearance to that in Sample B-3, but somewhat more tightly closed and therefore difficult to photograph. The third-harmonic background level was approximately -107 dBm, and the maximum third-harmonic flaw signal was approximately -82 dBm, which was 8 dB less than that

SAMPLE B-3
CRACK LENGTH = 0.182 in.

FIGURE 7 FATIGUE CRACK IN 2024-T3 ALUMINUM SAMPLE (X 500)

detected in Sample B-3. The second-harmonic background signal again was below the system sensitivity (-137 dBm). In this case, a weak second-harmonic flaw signal with an amplitude of approximately -125 dBm was detected.

Sample 2

This 6061 aluminum sample contained a single closed pseudo-crack (see Figure 8) that was produced by warm rolling at 500°C. The crack length is approximately 0.63 in. (16 mm) and its opening was 1-μm wide or less. The background signal at the third-harmonic frequency was approximately -107 dBm, and the maximum third-harmonic flaw signal was again strong and approximately equal to -74 dBm. The second-harmonic background signal was below system sensitivity (-137 dBm), and the pseudo-crack produced a weak second-harmonic signal of approximately -127 dBm.

SAMPLE 2
CRACK LENGTH ≃ 0.63 in.

FIGURE 8 PSEUDO-CRACK IN WARM-ROLLED 6061 ALUMINUM SAMPLE (X 200)

Sample 3

This 6061 aluminum sample also contained a single closed pseudo-crack (see Figure 9) that was produced by warm rolling at 500°C. In this case the crack length was approximately 0.31 in. (8 mm) and the crack opening was less than 0.5-μm wide. Again, the third-harmonic background level was approximately -107 dBm, and the maximum third-harmonic flaw signal was approximately -82 dBm. The second-harmonic flaw response was essentially the same as that observed in Sample C-3.

Sample 7

This 6061 aluminum sample contained two partially closed pseudo-cracks (see Figure 10) that were produced by cold rolling. The two cracks were separated by about 0.023 in. (0.6 mm). The longer of the two cracks was 0.18 in. (4.5 mm) in length, with a maximum opening width of 0.005 in. (0.14 mm). The other crack was 0.11-in. (2.8-mm) long,

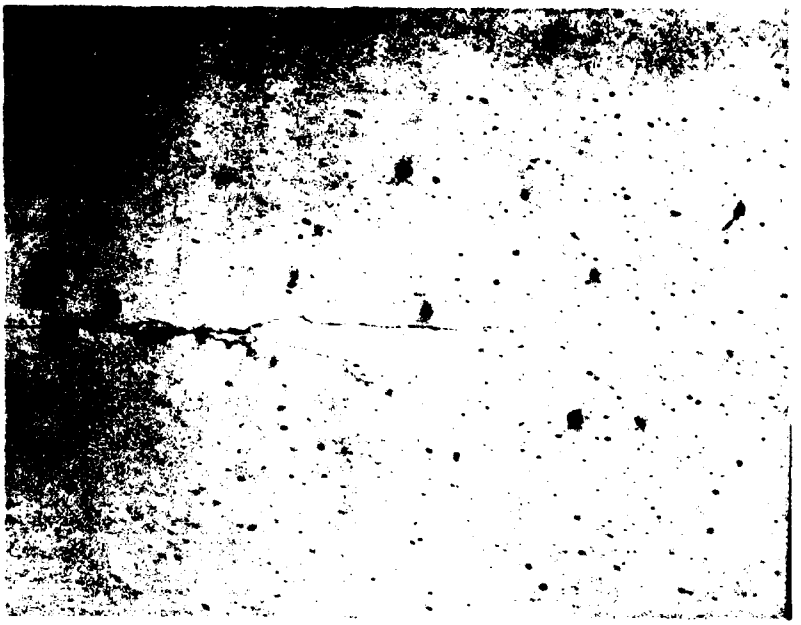

SAMPLE 3
CRACK LENGTH ≈ 0.31 in.

FIGURE 9 PSEUDO-CRACK IN WARM-ROLLED 6061 ALUMINUM SAMPLE (X 200)

with a maximum opening width of 0.004 in. (0.1 mm). The third-harmonic background level was approximately -107 dBm, and the maximum third-harmonic flaw signal was very large and approximately equal to -49 dBm. The second-harmonic flaw response was again the same as that observed in Sample 3.

Sample 8

This 6061 aluminum sample also contained two pseudo-cracks (Figure 11)--one closed, the other primarily open--both of which were produced by cold rolling. The two cracks were separated by 0.043 in. (1.1 mm). The longer of the two cracks was 0.185-in. (4.7-mm) long, with a maximum opening width of about 0.002 in. (0.06 mm). The other crack was 0.036-in. (2.2-mm) long, with a maximum opening width of 0.006 in. (0.16 mm). The third-harmonic background level was still approximately -107 dBm. However,

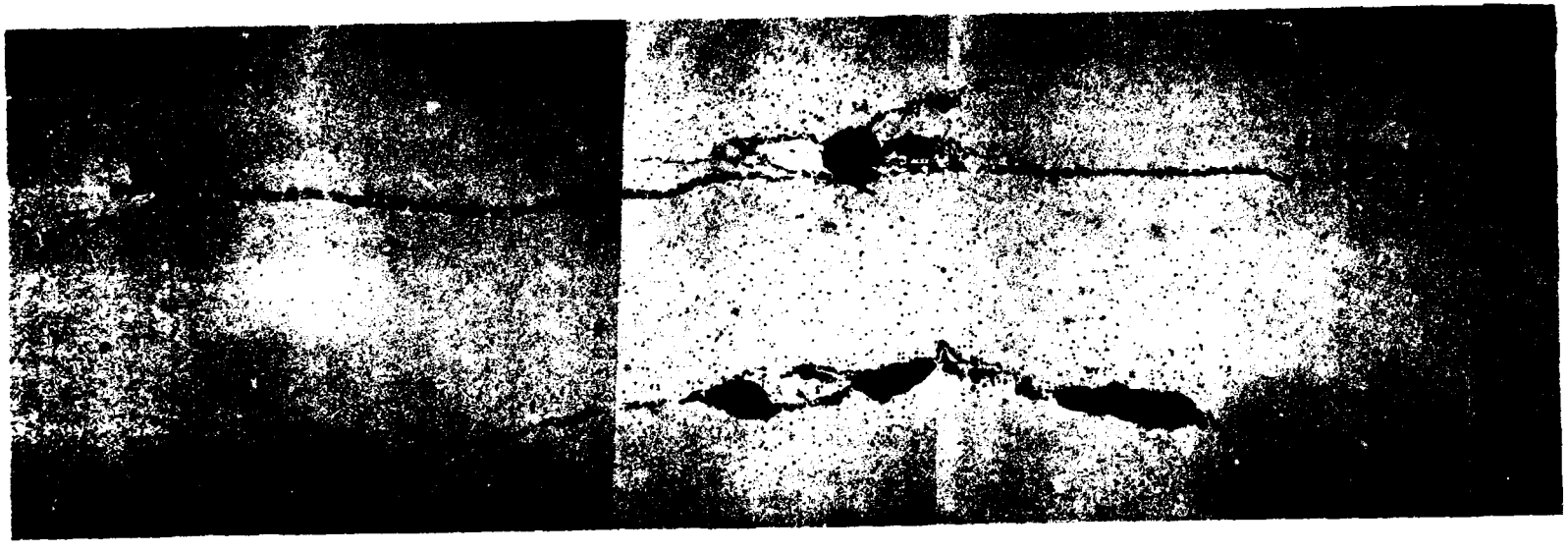

SAMPLE 7
CRACK LENGTHS = 0.18 in. and 0.11 in.

FIGURE 10 PSEUDO-CRACKS IN COLD-ROLLED 6061 ALUMINUM SAMPLE (X 50)

SAMPLE 8
CRACK LENGTHS = 0.185 in. and 0.086 in.

FIGURE 11 PSEUDO-CRACKS IN COLD-ROLLED 6061 ALUMINUM SAMPLE (X 50)

the maximum third-harmonic flaw signal was quite weak, having a level of approximately -100 dBm. The second-harmonic flaw response was again very similar to those observed in the other aluminum samples.

b. Copper Samples

Sample 9

This copper sample contained a single pseudo-crack (see Figure 12) that was produced by hot rolling. The crack was 0.165-in. (4.2-mm) long, with a maximum opening of 0.008 in. (0.21 mm). The third-harmonic background level for copper was observed to be approximately -101 dBm, which was slightly higher than that for aluminum. The maximum third-harmonic flaw signal was approximately -76 dBm. The background level at the second harmonic was below the system sensitivity (-137 dBm). A small second-harmonic flaw signal was detected which was very similar to those detected in the aluminum samples.

SAMPLE 9
CRACK LENGTH = 0.165 in.

FIGURE 12 PSEUDO-CRACK IN HOT-ROLLED COPPER SAMPLE (X 20)

Sample 10

This copper sample also contained a single pseudo-crack (see Figure 13) that was produced by hot rolling. The crack was 0.280-in. (7.1-mm) long, with a maximum opening of 0.014 in. (0.35 mm). The third-harmonic background level was approximately -101 dBm, and the maximum third-harmonic flaw signal was approximately -87 dBm. The maximum second-harmonic flaw signal was again very small.

SAMPLE 10
CRACK LENGTH = 0.280 in.

FIGURE 13 PSEUDO-CRACK IN HOT-ROLLED COPPER SAMPLE (X 14)

3. Discussion of Results

These results show that sensitivity to a crack nonlinearity is dramatically increased by using resonant probes operating between 1 and 3 GHz. We have shown unequivocably for the first time (to the best of our knowledge) that a third-order nonlinearity can exist in a surface-breaking fatigue crack in an aluminum plate (samples B-3 and C-3), the detected signals being 20 to 30 dB above the spurious third-harmonic

background level. Large third-harmonic flaw signals also were detected for pseudo-cracks in copper.

On the other hand, the second-harmonic flaw responses that were detected in these materials were always much weaker (typically only 10 dB above noise). Also, the variation of the second-harmonic flaw responses was not very great for different samples. These data characteristics make us hesitant to conclude that the second-order nonlinearity which we detected was indeed crack related.

In the following section we review the theoretical model for a nonlinear crack and present some calculations of its third-harmonic response at a frequency of 3 GHz.

IV THEORETICAL MODEL FOR A NONLINEAR CRACK

A. Nonlinear Response

Since we assume that the frequencies are low enough so that radiation from the crack is negligible, it seems reasonable to assume that the lumped equivalent-circuit model shown in Figure 14 can be used. In this circuit, Y_F is the flaw admittance associated with the crack in the absence of any nonlinearity, and C, G_0, and I_{NL} are the capacitance, conductance, and nonlinear current, respectively, of the nonlinear contact that is assumed to exist across the crack mouth. It is also assumed that the nonlinear current can be represented in the time domain by a power series:

$$i_{NL}(t) = \sum_{n=1}^{\infty} a_n v_2^n(t) \quad . \tag{1}$$

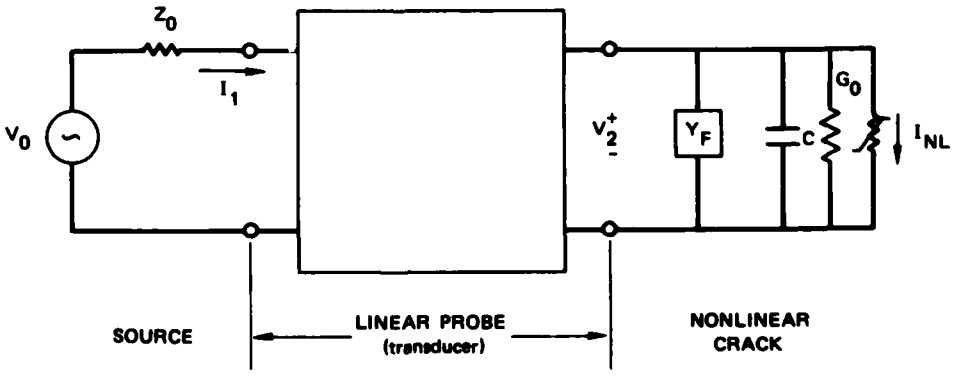

FIGURE 14 EQUIVALENT-CIRCUIT MODEL FOR SOURCE, PROBE, AND NONLINEAR CRACK

If the nonlinearity is weak (i.e., if the nonlinear coefficients, a_n, are small) this circuit can be analyzed using the Volterra-series approach described by Bussgang, et al.[10] Only the results of that analysis are presented here.

A Volterra-series analysis provides explicit frequency-domain expressions for the nonlinear currents I_{NL}, where the nonlinear current that corresponds to each harmonic or intermodulation frequency can be considered an independent current source that drives the circuit at that frequency. Thus, explicit expressions for the response currents, I_1, can be derived for each harmonic or intermodulation frequency. For example, the expression for the second-harmonic response current due to excitation at frequency f is

$$I_1(2f) = \frac{1}{2}a_2 V_0^2(f) K_v^2(f) K_v(2f) \quad , \tag{2}$$

where

$$K_v(f) = \frac{\phi(f) Y_{out}(f)}{Y_{out}(f) + Y_T(f)} \quad . \tag{3}$$

Here, $\phi(f)$ is the open-circuit output voltage of the probe obtained when $V_0(f) = 1$, and $Y_{out}(f)$ is the output admittance of the probe. The quantity $Y_T(f)$ is the total admittance of the crack, namely,

$$Y_T(f) = Y_F(f) + G_0 + j2\pi fC \quad . \tag{4}$$

Similarly, for two-frequency excitation, the second-order intermodulation response at the difference frequency is

$$I_1(f_1 - f_2) = a_2 V_0(f_1) V_0^*(f_2) K_v(f_1) K_v^*(f_2) K_v(f_1 - f_2) \quad , \tag{5}$$

where the asterisk (*) indicates complex conjunction.

A very useful feature of this analysis is that it shows explicitly how the admittances of the probe and crack at the fundamental, harmonic, and intermodulation frequencies affect the nonlinear responses at those frequencies.

If, for simplicity, we assume that $a_2 = 0$, the corresponding third-order responses are:

$$I_1(3f) = \frac{1}{4}a_3 V_0^3(f) K_v^3(f) K_v(3f) \quad , \tag{6}$$

and

$$I_1(2f_2 - f_1) = \frac{3}{4}a_3 V_0^*(f_1) V_0^2(f_2) K_v^*(f_1) K_v^2(f_2) K_v(2f_2 - f_1) \quad . \tag{7}$$

B. Flaw Impedance

The flaw impedance, $Z_F = 1/Y_F$, is related to the change in impedance, ΔZ_c, that is produced in an eddy-current probe as it passes over a flaw. Thus, to determine Z_F, we need first to derive an expression for ΔZ_c.

One effective method for calculating ΔZ_c is based on the Lorentz reciprocity theorem.[12] Application of this method to eddy-current problems has been discussed extensively by Auld.[13,14] Basically, the reciprocity theorem relates the change in impedance produced by a flaw to an integral of certain electromagnetic fields on the surface of a volume that encloses the flaw. One form of the mathematical expression for this theorem is

$$\Delta Z_c = \frac{1}{II'} \iint_{S_F} [(\tilde{n} \times \vec{E}') \cdot \vec{H} - (\tilde{n} \times \vec{E}) \cdot \vec{H}'] \, dS \quad , \tag{8}$$

where I is the current in the probe, $\tilde{n}$ is a unit vector pointing into the volume enclosed by the surface S_F, $\vec{E}$ is the electric field, and $\vec{H}$

is the magnetic field. The unprimed quantities correspond to the case of no flaw, while the presence of a flaw is indicated by a prime.

It is convenient to rewrite Eq. 8 in terms of the surface impedance, Z_s, where Z_s is defined by the relation

$$\tilde{n} \times \vec{E} = Z_s \vec{H}_t \quad , \tag{9}$$

where $\vec{H}_t$ is the component of $\vec{H}$ tangentical to the metal surface. If the radius of curvature at any point on the surface of the unflawed body is much greater than a skin depth, Z_s, is given by the well-known expression

$$Z_s = \frac{1}{Y_s} = (1 + j)\, R_s \quad , \tag{10}$$

where

$$R_s = \frac{1}{\sigma\delta} \quad . \tag{11}$$

Here, σ is the conductivity of the metal at σ is the skin depth.

As a further convenience, the magnetic fields can be normalized to the complex amplitude of the applied magnetic field, H_0:

$$\vec{h} = \frac{\vec{H}}{H_0} \quad , \tag{12}$$

and define

$$\vec{m}' = \frac{(\tilde{n} \times \vec{E}')}{H_0} \quad . \tag{13}$$

With these definitions, Eq. 8 becomes

$$\Delta Z_c = \frac{H_0^2}{II'} \iint_{S_F} \left[\left(\vec{m}' \cdot \vec{h} \right) - Z_s \left(\vec{h}_t' \cdot \vec{h}_t \right) \right] dS \quad . \tag{14}$$

Finally, let 2c be a characteristic dimension of the flaw such as crack length, and rewrite Eq. 14 as

$$\Delta Z_c = \left(\frac{2cH_0}{I} \right)^2 \cdot \frac{1}{(2c)^2} \iint_{S_F} \left[\left(\vec{m}' \cdot \vec{h} \right) - Z_s \left(\vec{h}_t' \cdot \vec{h}_t \right) \right] dS \quad , \tag{15}$$

or

$$\Delta Z_c = n_p^2 \cdot Z_F \quad , \tag{16}$$

where

$$n_p \triangleq \frac{2cH_0}{I} \quad , \tag{17}$$

and Z_F can be called the flaw impedance. It has been assumed for simplicity in Eq. 15 that $I = I'$. Note that the complex "turns ratio," n_p, is a strong function of lift-off. For example, if the probe is a very thin wire that is located a distance h above a highly conducting surface, one has $n_p \approx 2c/\pi h$. In addition, the flaw impedance, Z_F, is a function of lift-off because the spatial distribution of the applied fields depends on lift-off.

Equations 15 and 16 give the desired relationship between ΔZ_c and Z_F. Equation 15 is a rigorous expression for ΔZ_c; however, its evaluation requires that the fields with and without the flaw present be known. Alternatively, from a scattering point of view, one can

say that the incident and scattered fields must be known. In general, this is not a simple problem.

Fortunately, Auld et al[15] have obtained an approximate solution for the case of a uniformly excited slot having the shape of a circular arc, and which has length 2c, width Δu, and depth a. The result (assuming $a/\delta >> 1$) is

$$Z_F = 2R_s\left\{\frac{\bar{a}}{2c} - \frac{1}{n}\cdot\frac{\Delta u}{2c} + j\left[\frac{\bar{a}}{2c}\left(1 + S\cdot\frac{\Delta u}{2c}\right) - \frac{1}{n}\cdot\frac{\Delta u}{2c}\right]\right\} \quad , \tag{18}$$

where

$$n = 2 + \frac{4}{\pi}\tan^{-1}\left(\frac{a}{c}\right) \quad , \tag{19}$$

$$\frac{\bar{a}}{2c} = \int_{-1}^{1} F(x,n)\,dx \quad , \tag{20}$$

$$F(x,n) = \frac{(1/2n)\sin(2\pi/n)}{\cosh\left[(2/n)\ell n\left(\frac{1+x}{1-x}\right)\right] - \cos(2\pi/n)} \quad , \tag{21}$$

and

$$S = \sqrt{2k\sigma\eta_0\sigma c} \quad . \tag{22}$$

In Eq. 22, k is 2π divided by the free-space wavelength and $\eta_0 = 120\pi$ is intrinsic impedance of free space.

The flaw impedance given by Eq. 18 is basically the sum of two different types of terms: one term can be called a skin-effect (or internal) impedance, and is just the impedance presented to a strip of current one skin-depth deep that travels around the slot; the other term is multiplied by the parameter S and can be called an external impedance, which, for slot depths of less than one-quarter wavelength, is an inductive reactance associated with energy storage in the slot. The skin-effect impedance is composed of equal real and imaginary parts and increases as the square root of frequency, while the external

inductive reactance increases linearly with frequency. Hence, at high frequencies the external reactance will dominate the skin-effect impedance, provided the slot is open.

The depth parameter for a circular-arc slot, n, varies between 2 and 4. If $\Delta u \ll \bar{a}$, which is usually the case, then Eq. 18 simplifies to

$$Z_F \simeq 2R_s\left(\frac{\bar{a}}{2c}\right)\left[1 + j\left(1 + S \cdot \frac{\Delta u}{2c}\right)\right] \quad . \tag{23}$$

C. Numerical Example

As an example, consider the half-penny-shaped slot depicted in Figure 15a. For this case, evaluation of Eq. 20 gives $\bar{a}/2c = 0.145$. Since we want this slot to be a model of the fatigue crack in aluminum sample B-3, we choose $2c = 4.62$ mm and $\sigma = 3.54 \times 10^4$ mho/mm. Hence, taking $f = 1$ GHz, we find that $S = 1.73 \times 10^3$ and $R_s = 1.05 \times 10^{-2}\,\Omega$. Finally, if we take $\Delta u = 2.5 \times 10^{-2}$ mm, we have $\Delta u/2c = 5.4 \times 10^{-3}$. Thus,

$$Z_F = 3.04 \times 10^{-3} + j\ 3.15 \times 10^{-2} \text{ ohm} \quad , \tag{24a}$$

or

$$Y_F = 3.04 - j\ 31.45 \text{ mho} \quad . \tag{24b}$$

Next, consider the parameters of the nonlinear junction whose geometry is shown in Figure 15b. We assume that the contact is uniform so that the capacitance of this junction is given by the simple parallel-plate formula

$$C = \frac{\epsilon_r \epsilon_0 2c\Delta s}{\Delta t} \tag{25}$$

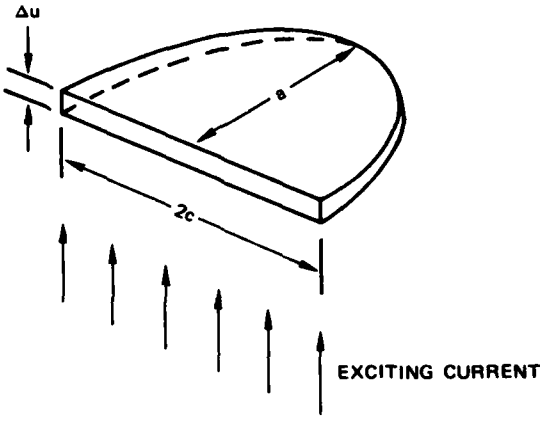

(a) HALF-PENNY GEOMETRY

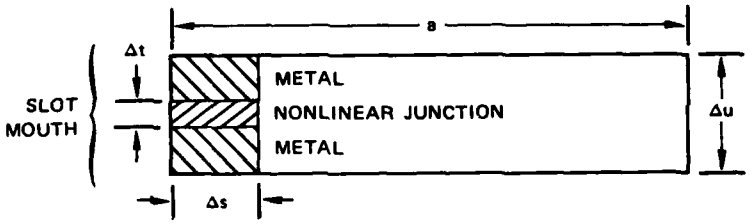

(b) SIDE VIEW OF NONLINEAR JUNCTION IN SLOT MOUTH

FIGURE 15 GEOMETRY OF HALF-PENNY SLOT CONTAINING NONLINEAR JUNCTION

where $\varepsilon_0 = 8.854 \times 10^{-15}$ F/mm and ε_r is the relative dielectric constant of the oxide in the junction. For aluminum oxide we take $\varepsilon_r = 10$, so that

$$C = 4.09 \times 10^{-13} \frac{\Delta s}{\Delta t} \quad . \tag{26}$$

Since Δt is typically $\approx 3 \times 10^{-6}$ mm,[4] and we assume that $\Delta s \leq \Delta u$, we have

$$C \leq 3.4 \times 10^{-9} F \quad . \tag{27}$$

Finally, the conductance and third-order nonlinear coefficient* for such a uniform junction have been measured by Bond et al.[4] They are:

$$G_0 = 2.7 \times 10^{-4} 2c\Delta s \text{ mho} \quad , \tag{28a}$$

and

$$a_3 = 3.0 \times 10^{-3} 2c\Delta s \text{ mho/V}^2 \quad , \tag{28b}$$

where 2c and Δs are in millimeters. Thus, in this example, we have $G_0 \leq 3.1 \times 10^{-5}$ mho and $a_3 \leq 3.4 \times 10^{-4}$ mho/V^2. We see that G_0 is negligible compared with the real part of Y_F (See Eq. 24b), and so the total slot admittance at 1 GHz becomes

$$Y_T = 3.04 - j(31.45 - 6.28 \times 10^9 C) \text{ mho} \quad . \tag{29}$$

If C is considered a variable parameter, parallel resonance of the slot would occur when $C = 5 \times 10^{-9}$F. The occurence of such a resonance would maximize the nonlinear harmonic response of the slot (see Eqs. 3 and 6). Note that this value of C is not very different from that calculated in Eq. 27.

To complete the calculation and find the power generated, say, at the third harmonic, we need a model for the probe. The required equivalent-circuit model fot the 1-GHz third-harmonic probe used in the experiments is shown in Figure 16. The part of this circuit designated "diplexer" is a filter circuit that separates the 1-GHz excitation from the 3-GHz response. The part of the circuit designated "probe" is a representation of the quarter-wave resonator that transforms the source impedance

*The second-order nonlinear coefficient is taken to be negligible for such a junction.

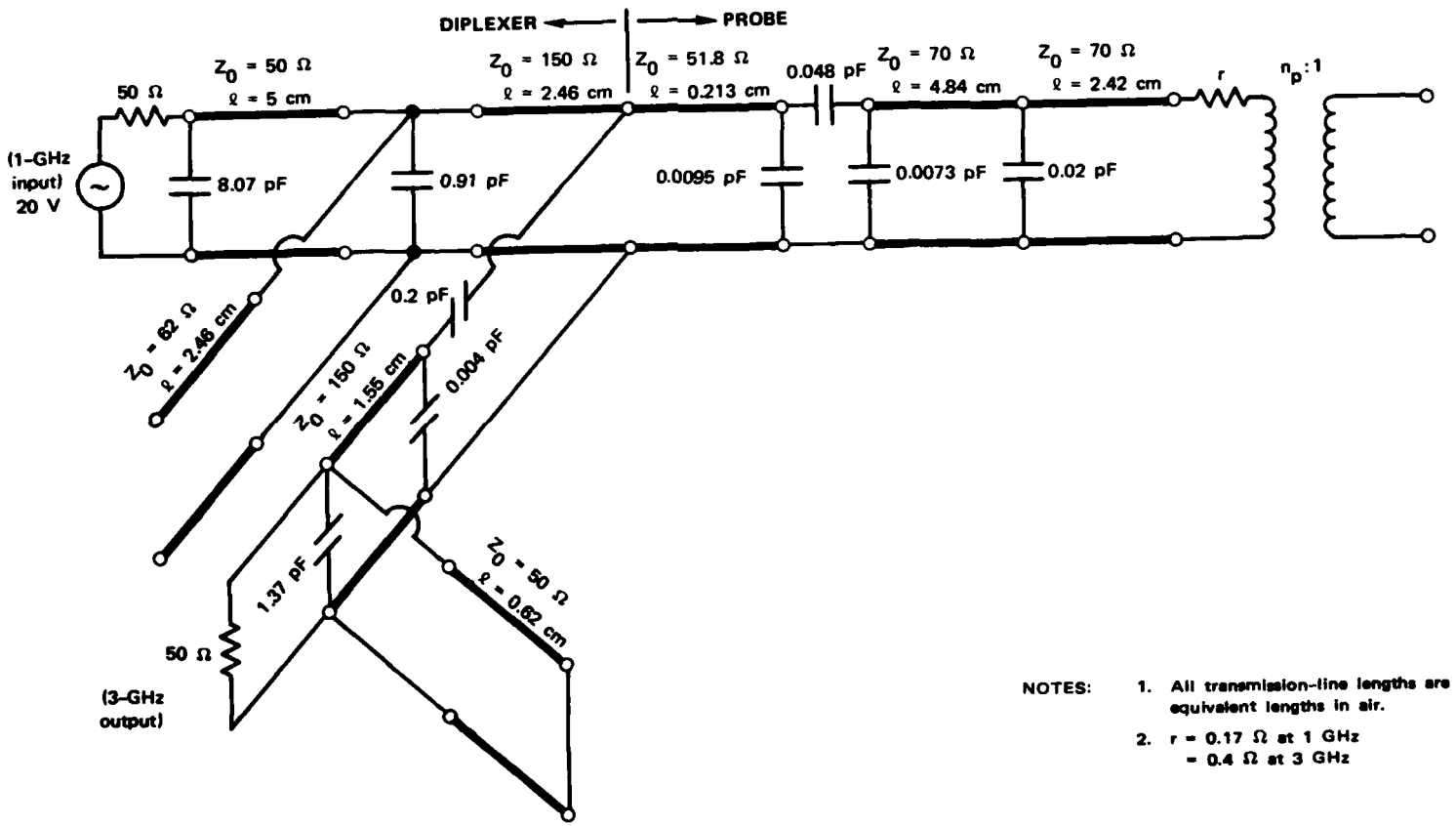

NOTES:
1. All transmission-line lengths are equivalent lengths in air.
2. r = 0.17 Ω at 1 GHz
   = 0.4 Ω at 3 GHz

FIGURE 16 EQUIVALENT CIRCUIT OF THIRD-HARMONIC PROBE

down to the low probe resistance, r. The ideal transformer with turns ratio, n_p, represents the magnetic coupling between the current that flows in the probe tip and the current that flows on the surface of the sample being tested. It is difficult to calculate n_p precisely, but we estimate that the value for the microstrip probe should be about an order of magnitude less than the value for a probe tip made of very thin wire, namely, $n_p = 2c/\pi h$, where h is the lift-off distance. In the calculations, therefore, we let n_p be a parameter that varies between, say, 0.5 and 4.

Calculations of the third-harmonic output power as a function of the contact depth, Δs, are shown plotted in Figure 17 and 18, with n_p as a parameter. The curves in Figure 17 were computed assuming an oxide thickness of 30 Å, while those in Figure 18 are for an oxide thickness of 10 Å. The sole effect of changing oxide thickness and contact depth is to change the contact capacitance, C. Therefore, these figures illustrate the high sensitivity of the third-harmonic output power to the value of this capacitance, which is a result of the slot-resonance effect mentioned above. The small peak seen in Figure 17 is a result of a slot resonance at 3 GHz, while the large peak seen in Figure 18 is a result of a slot resonance at 1 GHz. The resonance effect at 1 GHz is larger than the effect at 3 GHz because $K_v(f)$ is cubed in Eq. 6, while $K_v(3f)$ only appears to the first power.

The dependence of the third-harmonic output power on the transformer ratio, n_p, which is, in effect, a probe/flaw coupling parameter, is also illustrated in these figures. In general, increasing n_p increases the third-harmonic output power. However, when the slot is resonant at the fundamental frequency (see Figure 18), increasing n_p too much overcouples the resonator and the third-harmonic output power stops increasing proportionately and eventually begins to decrease.

Since the measured third-harmonic output power for sample B-3 was 4×10^{-8} mW, the calculated power clearly underestimates the measured power by several orders of magnitude. The most likely reasons for this lack of agreement are (1) use of an incorrect contact geometry in the model (the actual contact is probably made up of many point contacts

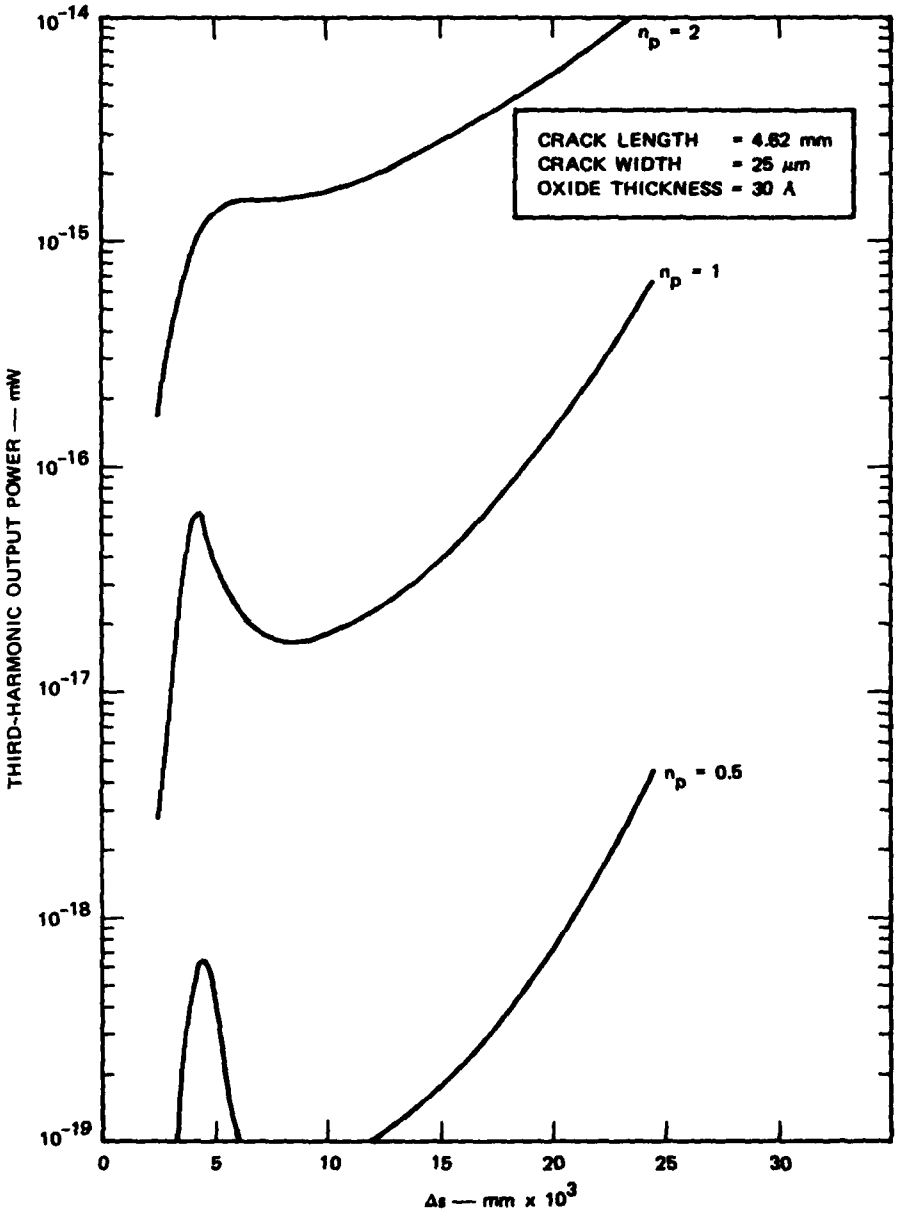

FIGURE 17 THIRD-HARMONIC OUTPUT POWER VERSUS CONTACT DEPTH FOR A HALF-PENNY SLOT IN ALUMINUM

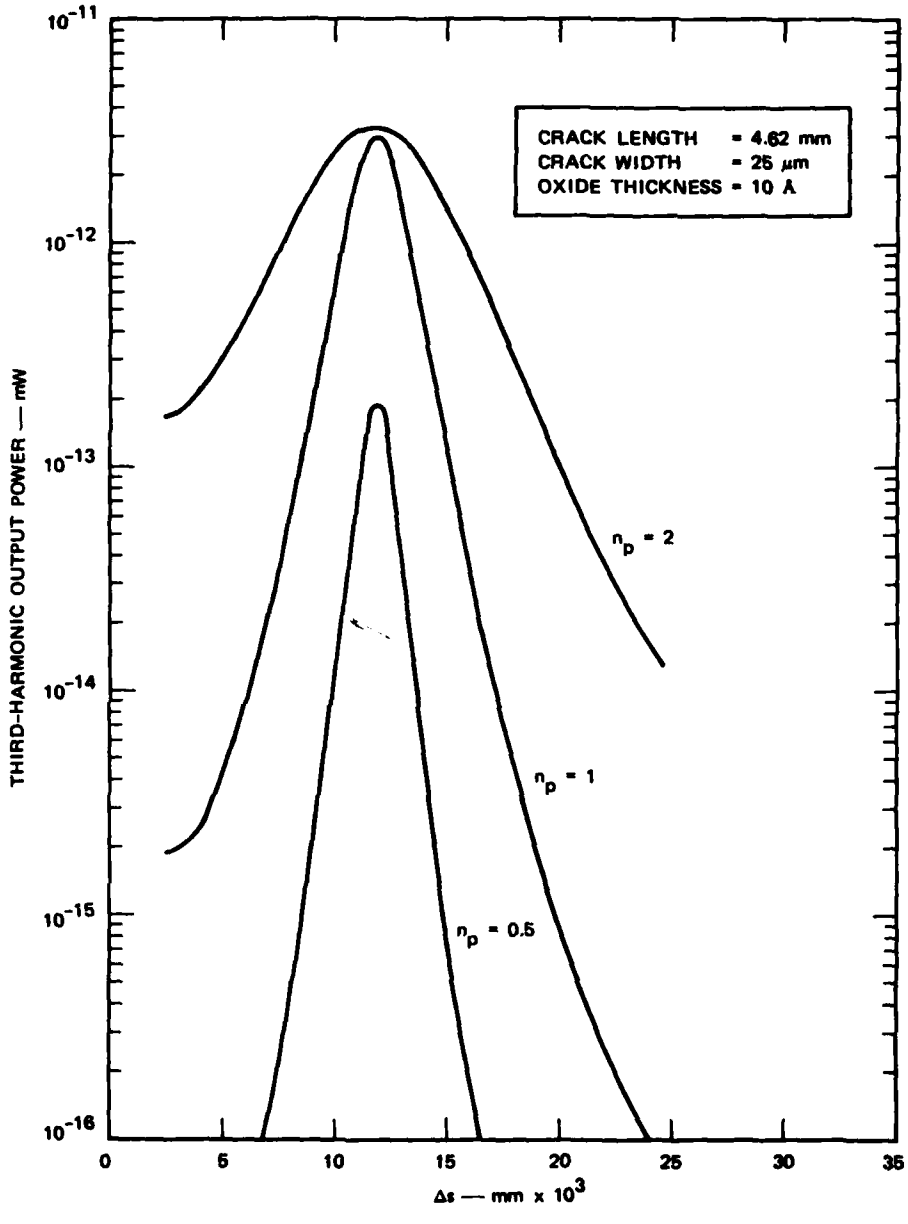

FIGURE 18 THIRD-HARMONIC OUTPUT POWER VERSUS CONTACT DEPTH FOR A HALF-PENNY SLOT IN ALUMINUM

rather than one continuous contact), (2) underestimation of the nonlinear coefficient, and (3) nonuniformity of the excitation currents produced by the probe. In fact, the model should almost certainly be stochastic rather than deterministic. Still, in spite of these failings, the simple deterministic model used here is useful for illustrating general dependencies of the nonlinear signal on probe and crack parameters.

V EXPERIMENTAL RESULTS FOR CRACKS IN MODIFIED COMPACT-TENSION SPECIMENS

To evaluate the performance of the third-harmonic probe in a more realistic environment, a series of fatigue tests was conducted in which this probe was used to monitor the initiation and growth of a fatigue crack in modified aluminum compact-tension specimens like that shown in Figure 19. During these tasks the signals from the third-harmonic probe were compared and correlated with crack initiation and growth data obtained from specimen compliance records.

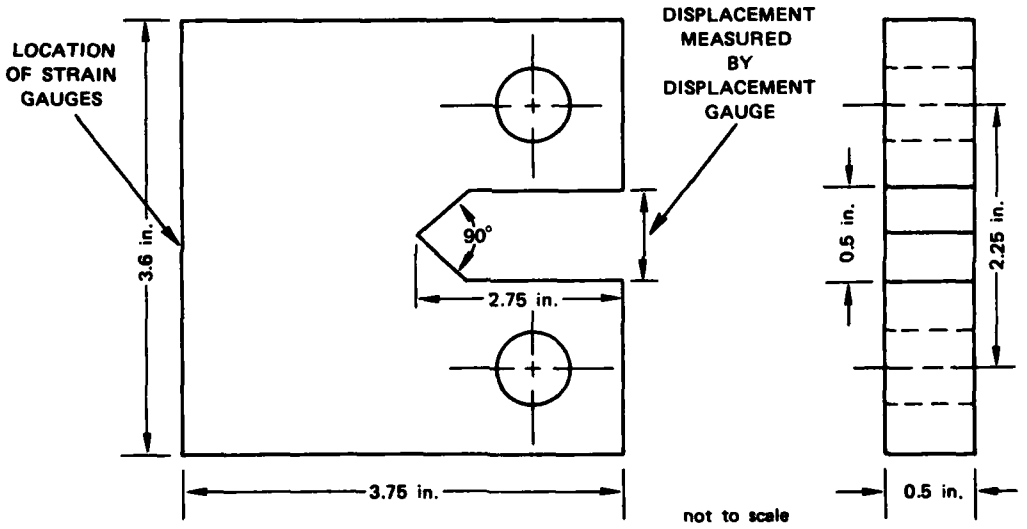

FIGURE 19 DIMENSIONS OF MODIFIED ALUMINUM COMPACT-TENSION SPECIMEN

The mechanical compliance of a specimen is the inverse of its stiffness and represents the displacement at a fixed location in the specimen resulting from the application of a unit load. The compliance increases monotonically with the depth of a crack in the specimen, and thus can be used to monitor crack growth. When a compliance-versus-crack-depth calibration curve is available, the crack depth can be evaluated at any stage of crack propagation by a simple compliance measurement.

In the present experiments, two types of compliance measurements were performed. In one case, we used a displacement gauge at the notch opening in the specimen to measure its deflection. In the other case, strain gauges were mounted on the back of the specimen to monitor back-face strains (Figure 19). The outputs of the strain and displacement gauges were recorded as functions of the applied load, and the slope of the resulting plots yielded the compliance.

The specimens were mounted in an MTS Model 911 closed-loop universal electrohydraulic testing machine. A fixture on which the third-harmonic microwave probe and a linear eddy-current microwave probe were mounted was attached to the stationary load cell. A photograph of this arrangement is shown in Figure 20.

The two microwave probes were attached to the fixture in a manner which allowed them to be carefully aligned with respect to the notch in the specimen. The fixture also incorporated two linear-translation stages that were connected to position-indicating potentiometers. These stages permitted each probe to be scanned across the notch with a minimum of lift-off variation. A photographic view of this fixture with the third-harmonic probe positioned in the notch is shown in Figure 21.

The measuring system whose block diagram is shown in Figure 6 was modified for these tests by adding a storage oscilloscope. The spectrum analyzer was used as a fixed-tuned receiver and was set to the third-harmonic frequency of the synthesized source. The video output of the spectrum analyzer was connected to the vertical amplifier of the storage oscilloscope, and the voltage derived from the probe-position potentiometers was used to drive the oscilloscope's horizontal amplifier. The resulting display was a plot of third-harmonic power as a function of the probe's position in the notch.

The measuring system used with the linear microwave eddy-current probe is described in detail elsewhere.[11] Our original thought was to use this linear probe to make measurements that could be compared with those obtained using the third-harmonic probe. However, the specimen geometry used in these tests precluded the use of this probe in its

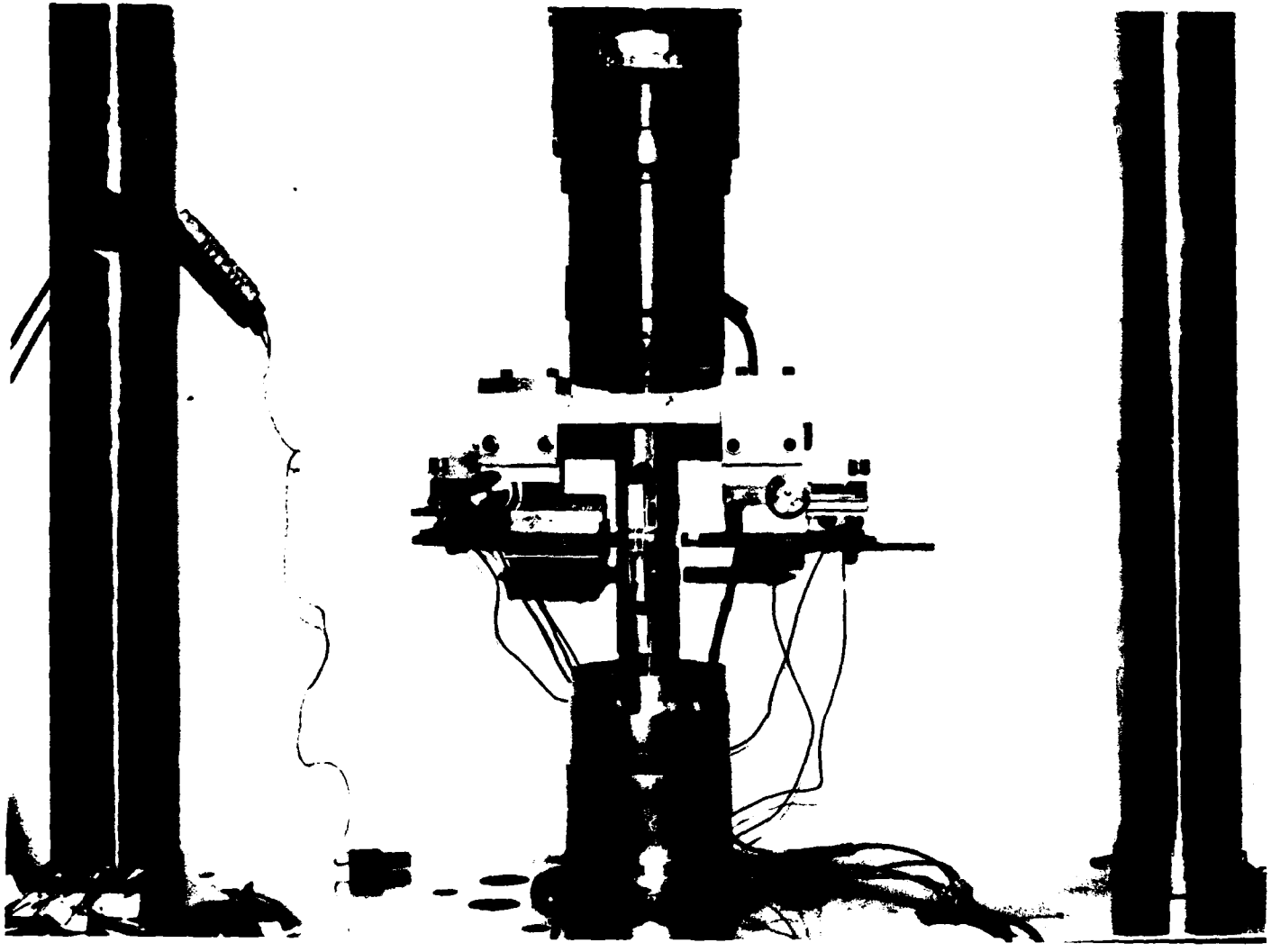

FIGURE 20 MTS UNIVERSAL TESTING MACHINE WITH MICROWAVE PROBES IN PLACE

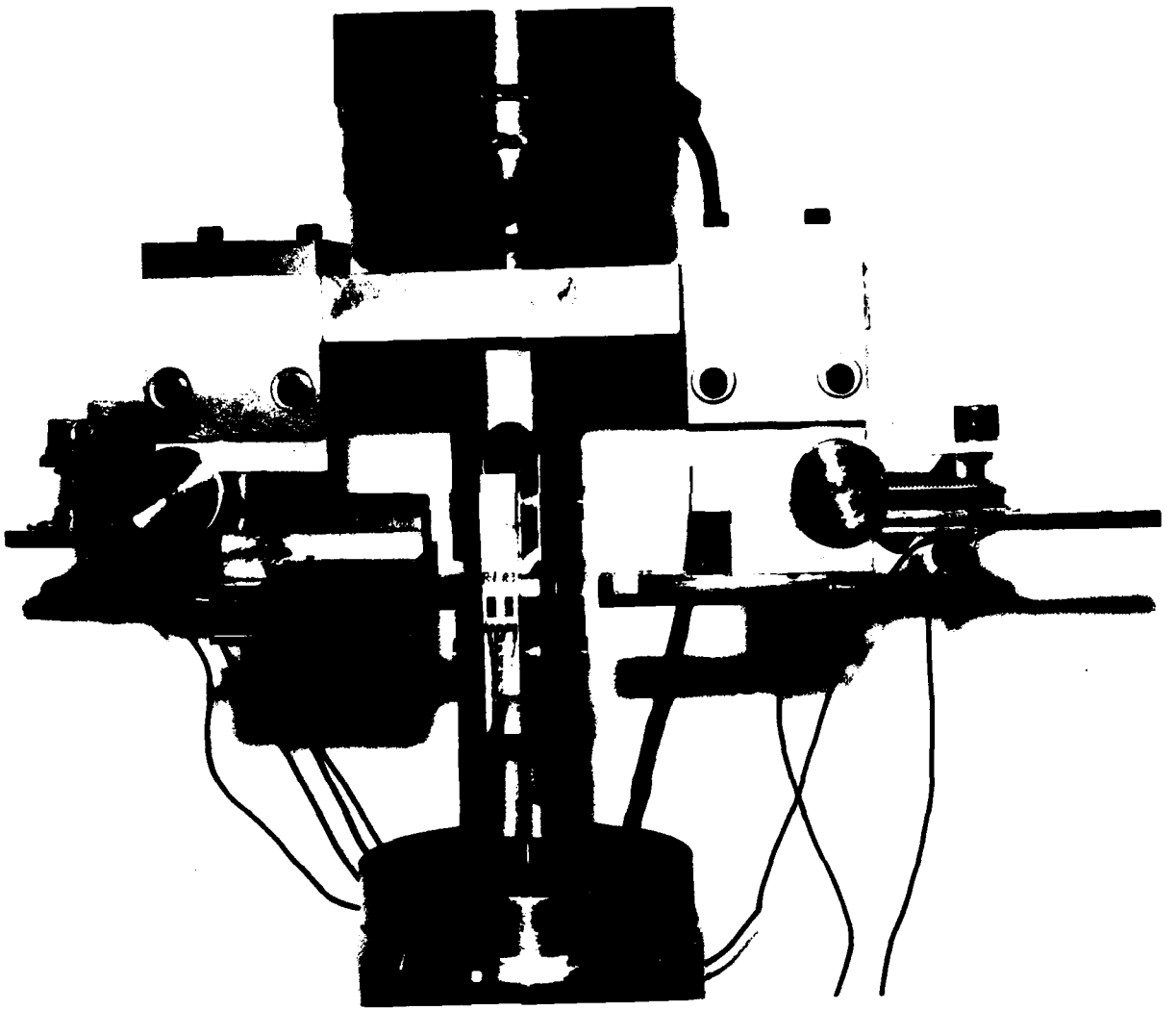

FIGURE 21 FIXTURE FOR MICROWAVE PROBES

differential form, and thus we implemented the linear probe as an absolute probe. This type of probe proved too sensitive to lift-off to be used to detect a small crack, and thus its use was abandoned early in the tests.

The microwave probes were constructed so that they conformed with the notch in the compact-tension specimens. The vertex of each probe was located in the center of the 0.010-in.-wide short-circuiting strip that forms the tip of the probe (Figure 3) in order to excite the notch as uniformly as possible. A close-up view of the tip of a notch-inspection probe (with insulating tape removed) is shown in Figure 22.

Two 7075-T6 aluminum specimens were tested. A sinusoidal force that varied between a maximum of 900 lb and a minimum of 250 lb (preload level) was applied during the tests at a frequency of 10 Hz. Compliance data, as well as the signal from the third-harmonic probe, were recorded every 1000 cycles at the preload level until the initiation of a crack was detected. One test was continued after crack initiation in order to monitor the third-harmonic signals that occurred during crack growth. For this test the data were taken every 500 cycles after crack initiation, and the maximum load was changed occassionally to control the growth rate of the crack.

In the first test, crack initiation was detected by the compliance technique first after roughly 26,000 cycles and then by the third-harmonic probe after a few more cycles. At that point the crack had grown to a depth of about 0.040 in. (1.0 mm). Figure 23a shows the third-harmonic background signal before the start of the test, and Figure 23b shows the changes in third-harmonic signal that indicate the presence of a crack. The third-harmonic background signal for this probe was about 10 dB larger than for the flat-plate probe discussed in Section III. The vertical sensitivity of oscilloscope display was about 5 dB/div, and the horizontal sensitivity was 0.125 in./div. Two particular aspects of this third-harmonic signal are worth noting. First, the third-harmonic signals were highly localized, indicating the nonlinear contacts were localized. Second, the crack signals represented a decrease in power, indicating that the crack signal was out of phase with the background signal.

FIGURE 22 CLOSE-UP VIEW OF NOTCH-INSPECTION PROBE TIP

(a) BACKGROUND SIGNAL BEFORE START OF FATIGUE TEST

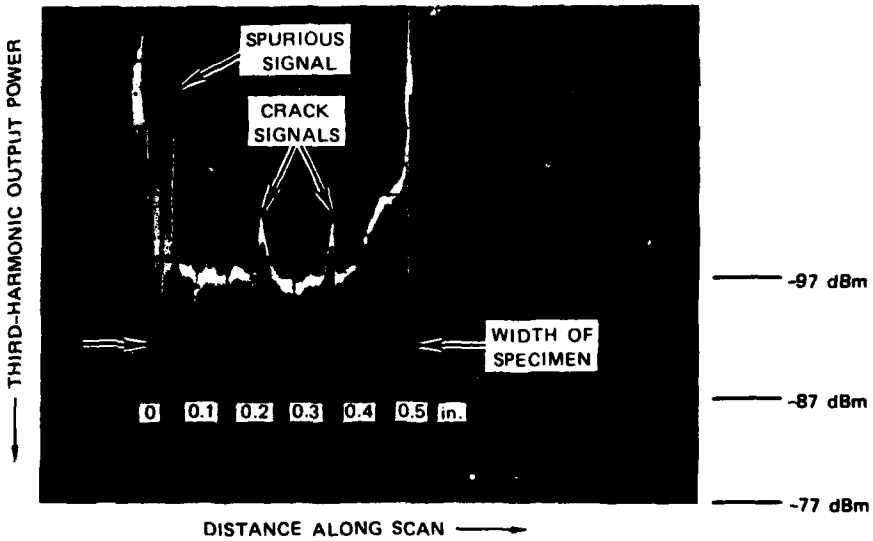

(b) CRACK RESPONSE AFTER 26,000 CYCLES

FIGURE 23 RESPONSE OF THIRD-HARMONIC PROBE TO A SHALLOW CRACK

After the crack had been detected with the third-harmonic probe, the cyclic loading was stopped and the specimen was broken open. A photograph of the region around the notch tip is shown in Figure 24. The light-colored strip emanating from the notch tip is the cracked region, which clearly extends all the way through the specimen. Unfortunately, there was no way to correlate any particular features of the crack-surface topology with the third-harmonic signals shown in Figure 23b.

FIGURE 24 SHALLOW CRACK IN A MODIFIED ALUMINUM COMPACT-TENSION SPECIMEN

To explain the source of the spurious signal indicated in Figure 23b, a few comments regarding the measurement procedure are needed. In these tests the probe surface was insulated with 0.0005-in.-thick Mylar tape to increase the coupling with the notched specimen over that which would be obtained with the 0.002-in.-thick Scotch tape that was used on the flat-plate probe discussed earlier. As the probe rubbed against the specimen, trace amounts of aluminum would adhere to the tape and to bits of adhesive which squeezed from the edges of the tape.

This contamination of the tape surface was removed frequently because, if left in place, it would have introduced noise. Also, other sources of noise occasionally appeared, but these sources were not identified. The crack signals were easily differentiated from the spurious signals by performing two or three scans. With each scan, the crack signals repeatedly appeared at the same location and with basically the same shape. However, the spurious signals came and went and appeared in different locations during each scan.

In the second test, a modified compact-tension specimen was subjected to a large number of loading cycles, and the third-harmonic signals were monitored at every 500 cycles after crack initiation. This test was very interesting in that the third-harmonic signals that were detected suggest that the crack growth occurs sporadically, rather than continuously.

A representative set of third-harmonic responses obtained during this extended test are shown in Figure 25. The crack was first detected by the third-harmonic probe after 30,000 cycles. The crack was also detected about the same time by the compliance technique, and, using the compliance data, the crack depth was estimated to be about 0.005 in. (0.127 mm).

The third-harmonic response was found to exhibit characteristic peaks at one measurement point, but after continued cycling the peaks would disappear and the response would return to that of an uncracked sample (see Figure 25a). Upon continued cycling the peaks would reappear (Figure 25b) and sometimes increase in amplitude (Figure 25c) before disappearing again (Figures 25d and 25e). After further cyclic loading, the crack signal would again reappear (Figure 25f). Sometimes the crack signals became quite large, as can be seen in Figure 26. This repetitive behavior suggests that the nonlinear junctions which are

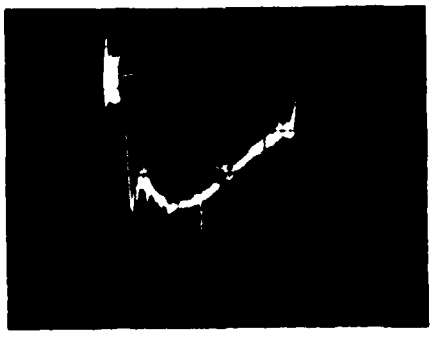

(a) 50,684 CYCLES

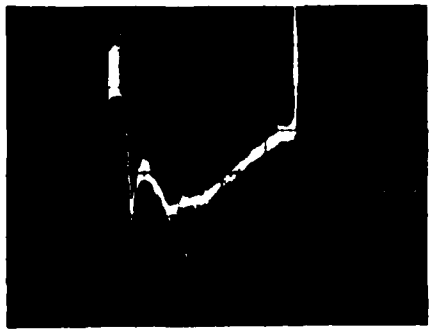

(d) 52,184 CYCLES

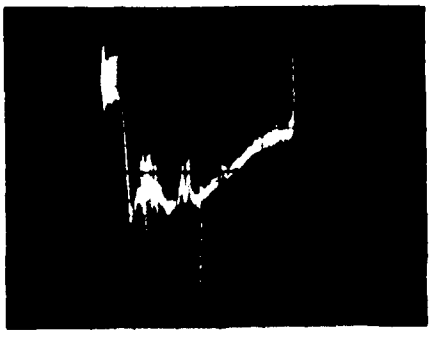

(b) 51,184 CYCLES

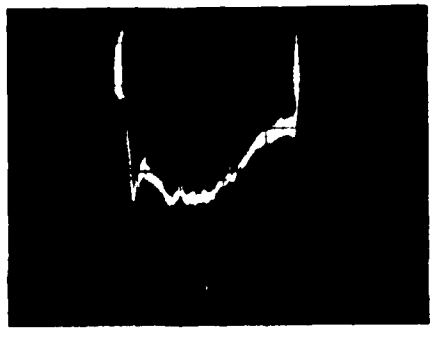

(e) 52,684 CYCLES

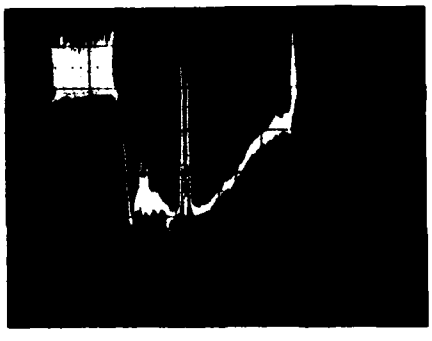

(c) 51,684 CYCLES

(f) 53,184 CYCLES

FIGURE 25 THIRD-HARMONIC CRACK RESPONSES OBSERVED DURING CRACK GROWTH

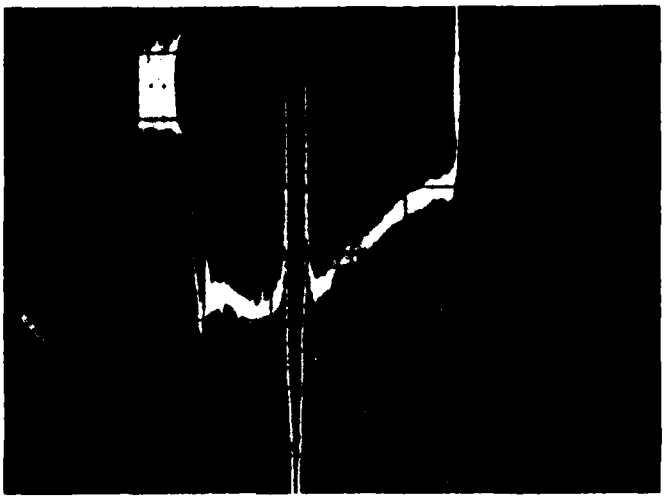

(a) AFTER 55,687 CYCLES

(b) AFTER 57,690 CYCLES

FIGURE 26 EXAMPLES OF LARGE THIRD-HARMONIC CRACK SIGNALS OBSERVED DURING CRACK GROWTH

formed after crack initiation are destroyed with continued cyclic loading, and that additional crack growth is needed before new nonlinear junctions are formed.

This hypothesis was tested by reducing the maximum load from 750 lb to 550 lb in order to retard or temporarily arrest the crack growth. Decreasing the crack-growth rate should reduce the number of new nonlinear junctions that are formed, and, hence, fewer third-harmonic crack signals should be observed. This reduced load was maintained for 4000 cycles, and little or no crack growth occurred. Consistent with the hypothesis, no new third-harmonic crack signals were observed. The load was then returned to 750 lb to reinitiate crack growth, and, indeed, a third-harmonic crack signal reappeared.

This test was terminated at 98,684 cycles and the specimen was broken open. Figure 27 shows a photograph of the region around the notch tip. Again, the light-colored area is the fatigue crack, and the dark band in that area is the portion of the crack where crack growth was the result of tearing produced by the static tensile stress applied during one of the mechancial compliance measurements.

The data obtained during this extended test using the third-harmonic probe and the compliance gauge are summarized in Figure 28. The photographs of the third-harmonic responses were reviewed, and each response was assigned a qualitative rating, namely "yes" for a crack detected, "no" for no crack detected, and "?" for an indeterminant response. In Figure 28, these qualitative ratings and the average crack depth determined from the compliance measurements are plotted versus the number of loading cycles. In general, it can be seen that high crack-growth rates correspond to the greatest incidence of third-harmonic signals. Thus, measurements of third-harmonic signals from cracks appear to offer a new (albeit qualitative) method for monitoring crack growth. The statistical nature of the formation of nonlinear contacts within a crack make this method roughly akin to crack-growth-monitoring methods based on acoustic emission.[16]

FIGURE 27 DEEP CRACK IN A MODIFIED ALUMINUM COMPACT-TENSION SPECIMEN

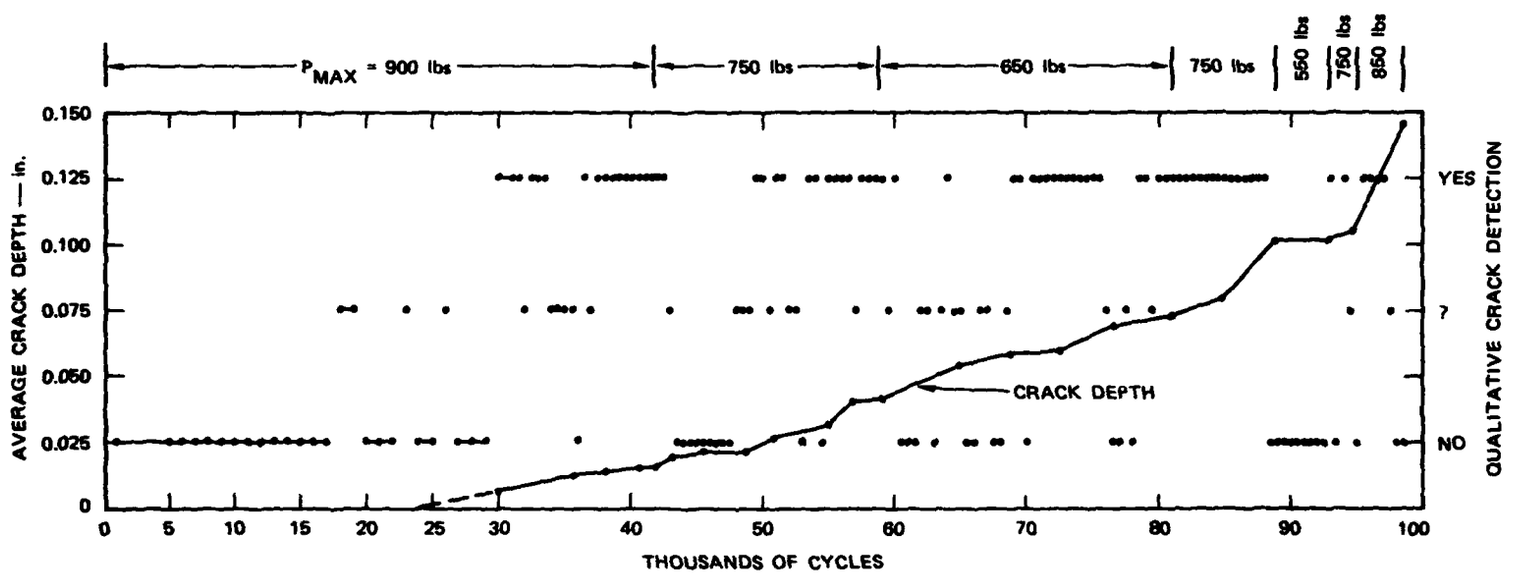

FIGURE 28 QUALITATIVE THIRD-HARMONIC RESPONSE AND AVERAGE CRACK DEPTH VERSUS NUMBER OF LOADING CYCLES

VI CONCLUSIONS

When we began this research there was no direct experimental evidence of the existence of any type of electromagnetic nonlinearity within a surface-breaking crack in a conducting material. We have shown that such nonlinearities can exist and can be detected. In the samples we tested, the third-order signals were always much larger than the second-order signals, suggesting that the source of these signals was a symmetrical nonlinear junction. This conclusion is consistent with the view that the source of the nonlinearity is a metal-oxide-metal junction, and, hence, that the ability of the material to oxidize is a necessary material characteristic if such junctions are to form.

One of the major objectives of this research was to develop a reliable detector of closed cracks. Unfortunately, this nonlinear crack-detection technique cannot be said to be reliable for two main reasons. First, the nonlinear signals generated by cracks are weak, and therefore are easily masked by spurious background signals, such as those generated by poor contacts inside the probe or by other nonlinear properties of the material (e.g., the nonlinear permeability of a ferrous material). Second, nonlinear contacts do not always exist in a crack, or they may come and go as the crack grows.

Another objective of this work was to develop a quantitative relationship between the amplitude of the nonlinear signal produced by a crack, its size, or some other strength-related parameter. Although our crack model was crude, it showed that the amplitude of the nonlinear signal is strongly dependent on junction area and thickness, both of which can be expected to vary widely among the contacts in a real fatigue crack. It cannot be expected, therefore, that a deterministic crack model like the one described in this report would yield the desired accurate quantitative relationship. Any future work in this area should seek to develop a stochastic model for the nonlinear junction inside a crack.

The results obtained by using a third-harmonic probe to monitor the growth of a crack in a modified compact-tension specimen suggest that this technique can yield information on the rate of crack growth. Such a technique could be important in studying mechanisms of crack growth, and perhaps even in detecting crack growth in actual engineering structures.

In conclusion, it should be re-emphasized that the nonlinear response of a crack is very strongly dependent on the magnitude of its impedances at the frequencies involved in the measurement. Frequencies in the low microwave range appear to be about optimum with respect to producing the largest crack impedances, and, hence, the largest nonlinear response.

REFERENCES

1. R. Elsner et al., "Engineering Study for Electrical Hull Interaction," Final Report, Contract No. N123953 35417A (January 1965) AD462979.

2. T. R. Pound et al., "Research on Natural and Ferromagnetic Nonlinearities," Final Report, Contract No. DAAK02-70-C-0028 (July 1971) CONFIDENTIAL AD519758.

3. W. Higa, "Spurious Signals Generated by Electron Tunneling on Large Reflector Antennas," Proc. IEEE, Vol. 63, pp. 306-313 (February 1975).

4. C. D. Bond, C. S. Guenzer, and C. A. Carosella, "Intermodulation Generation by Electron Tunneling Through Aluminum-Oxide Films," Proc. IEEE, Vol. 67, pp. 1643-1652 (December 1979).

5. C. L. Opitz, "Metal-Detecting Radar Rejects Clutter Naturally," Microwave, Vol. 15, pp. 12-14 (August 1976).

6. V. Peterson and P. Harris, "Harmonic Testing Pinpoints Passive Component Flaws," Electronics, pp. 93-100 (11 July 1966).

7. N. I. Meyer and T. Guldbrandsen, "Method for Measuring Impurity Distributions in Semiconductor Crystals," Proc. IEEE, Vol. 51, pp. 1631-1637 (November 1963).

8. A. J. Bahr, "Microwave Detection of Third-Order Nonlinearities in Fatigue Cracks," Electronics Letters, Vol. 16, pp. 150-152 (February 1980).

9. B. A. Auld, F. Muennemann, and D. K. Winslow, "Surface Flaw Detection with Ferromagnetic Resonance Probes," Proceedings of the DARPA/AF Review of Progress in Quantitative NDE, La Jolla, California (July 1980).

10. J. J. Bussgang, et al., "Analysis of Nonlinear Systems with Multiple Inputs," Proc. IEEE, Vol. 62, pp. 1088-1118 (August 1974).

11. A. J. Bahr and J. P. Watjen, "Novel Eddy-Current Probe Development," Final Report, Contract F33615-80-C-5025, SRI International, Menlo Park, California (September 1981).

12. R. E. Collin, Field Theory of Guided Waves, New York: McGraw-Hill, pp. 39-40 (1960).

REFERENCES (Concluded)

13. B. A. Auld, "Theory of Ferromagnetic Resonance Probes for Surface Cracks in Metals," G. L. Report 2839, Ginzton Laboratory, Stanford University, Stanford, California (July 1978).

14. B. A. Auld, "Theoretical Characterization and Comparison of Resonant-Probe Microwave Eddy-Current Testing with Conventional Low-Frequency Eddy-Current Methods," Eddy-Current Characterization of Materials and Structures, ASTM STP 722, G. Birnbaum and G. Free, eds., American Society for Testing and Materials, pp. 332-347 (1981).

15. B. A. Auld, F. Muennemann, and D. K. Winslow, "Observation of Fatigue Crack Closure Effects with the Ferromagnetic Resonance Eddy-Current Probe," G. L. Report 32^3, Ginzton Laboratory, Stanford University, Stanford, California (March 1981).

16. "Monitoring Structural Integrity by Acoustic Emission," American Society for Testing and Materials, Special Technical Publication No. 571, Philadelphia, Pennsylvania (1975).

Appendix

THIRD-HARMONIC RESPONSES FOR CRACKS IN FLAT SAMPLES

Appendix

THIRD-HARMONIC RESPONSES FOR CRACKS IN FLAT SAMPLES

The following data for flat samples were obtained by photographing the display on an HP spectrum analyzer consisting of a 141S display section, an 8555A RF section, and an 8552B IF section. The control settings on the spectrum analyzer were as follows (except where noted in the figures):

Bandwidth = 1 kHz
Scanwidth = 5 kHz/div
RF attenuation = 20 dB
Scan time = 5 ms
Log reference level = -20 dBm
Video filter = OFF
Vertical gain = 10 dB/div.

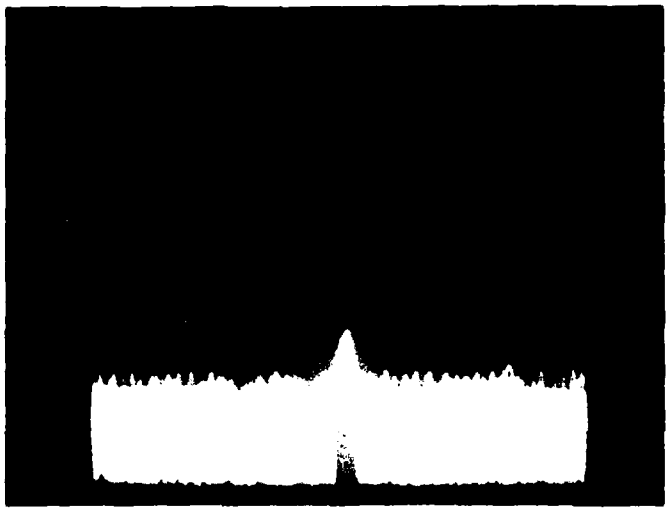

*Log reference level is -20 dBm, but the spectrum analyzer is preceded by a preamplifier with approximately 37 dB of gain.

FIGURE A-1 THIRD-HARMONIC BACKGROUND SIGNAL LEVEL FOR ALUMINUM SAMPLES

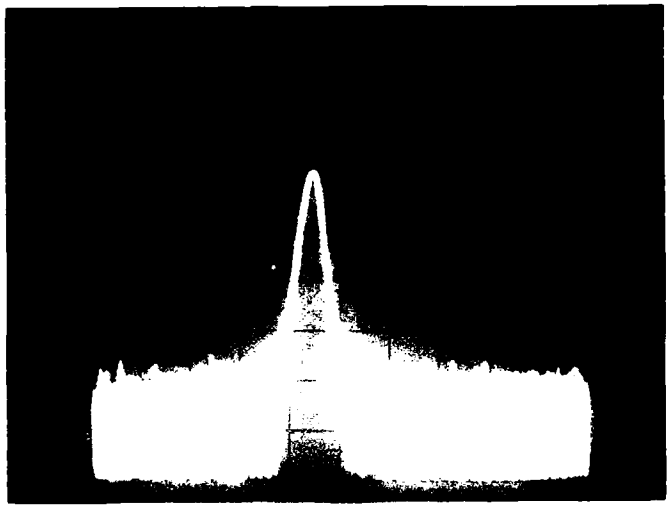

FIGURE A-2 MAXIMUM THIRD-HARMONIC SIGNAL FROM A FATIGUE CRACK IN ALUMINUM SAMPLE B-3

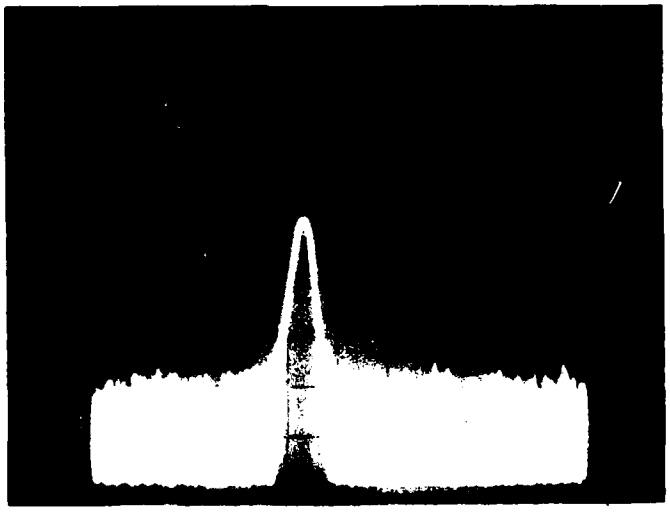

FIGURE A-3 MAXIMUM THIRD-HARMONIC SIGNAL FROM A FATIGUE CRACK IN ALUMINUM SAMPLE C-3

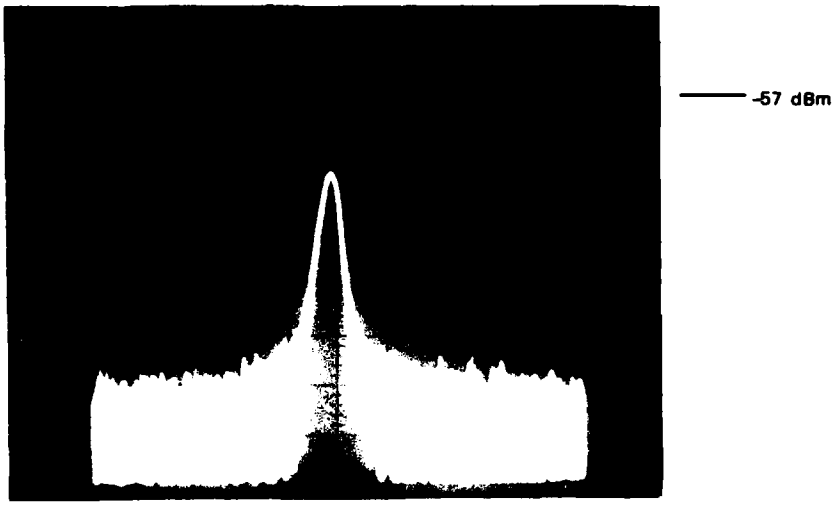

FIGURE A-4 MAXIMUM THIRD-HARMONIC SIGNAL FROM A PSEUDO-CRACK IN ALUMINUM SAMPLE 2

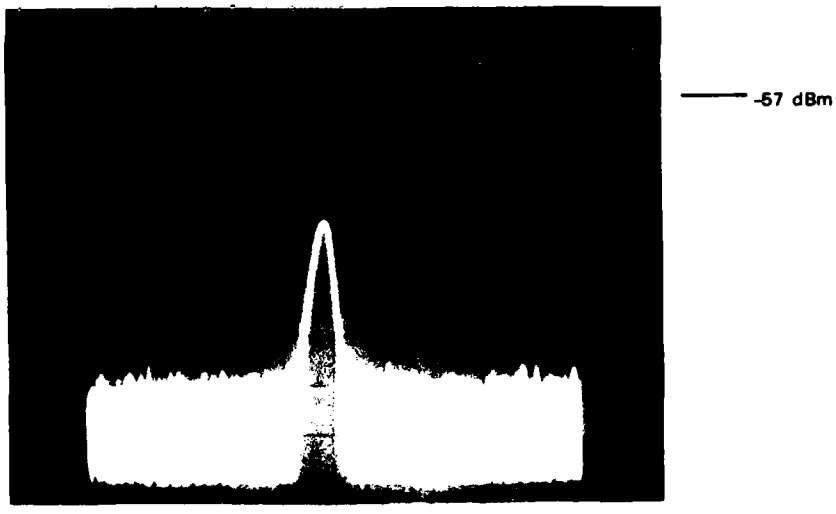

FIGURE A-5 MAXIMUM THIRD-HARMONIC SIGNAL FROM A PSEUDO-CRACK IN ALUMINUM SAMPLE 3

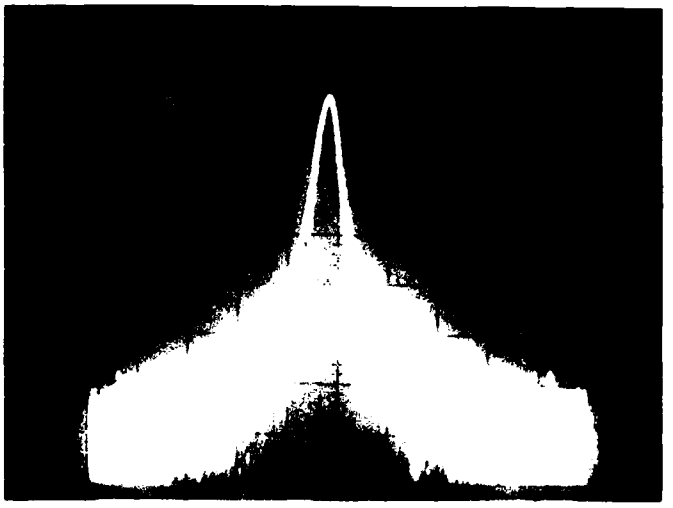

FIGURE A-6 MAXIMUM THIRD-HARMONIC SIGNAL FROM A PSEUDO-CRACK IN ALUMINUM SAMPLE 7

FIGURE A-7 MAXIMUM THIRD-HARMONIC SIGNAL FROM A PSEUDO-CRACK IN ALUMINUM SAMPLE 8

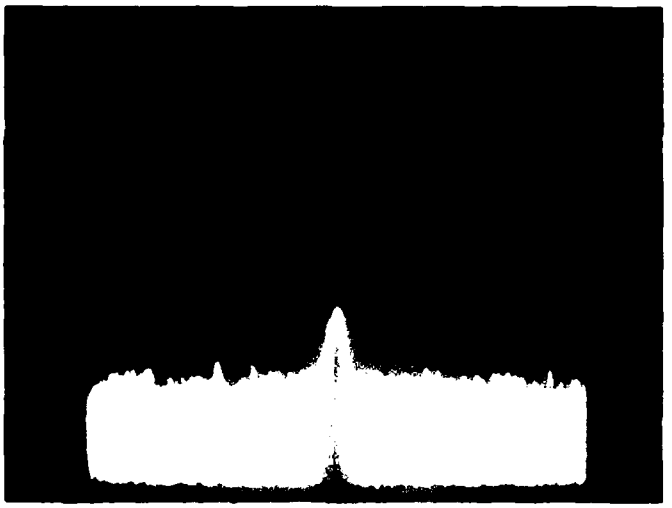

FIGURE A-8 THIRD-HARMONIC BACKGROUND SIGNAL LEVEL FOR COPPER SAMPLES

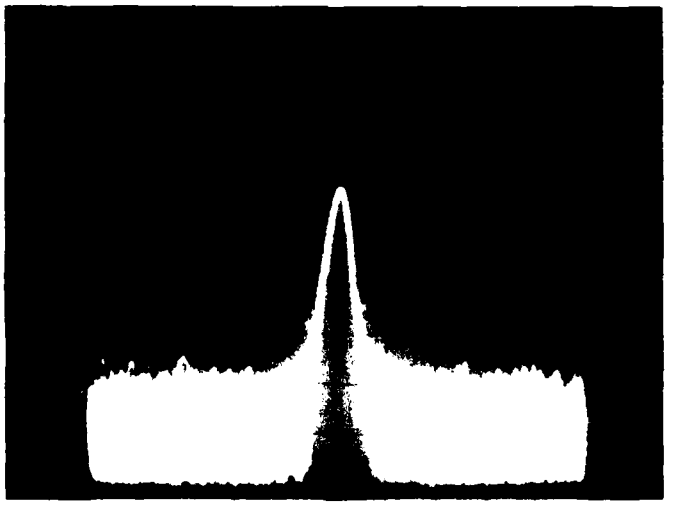

FIGURE A-9 MAXIMUM THIRD-HARMONIC SIGNAL FROM A PSEUDO-CRACK IN COPPER SAMPLE 9

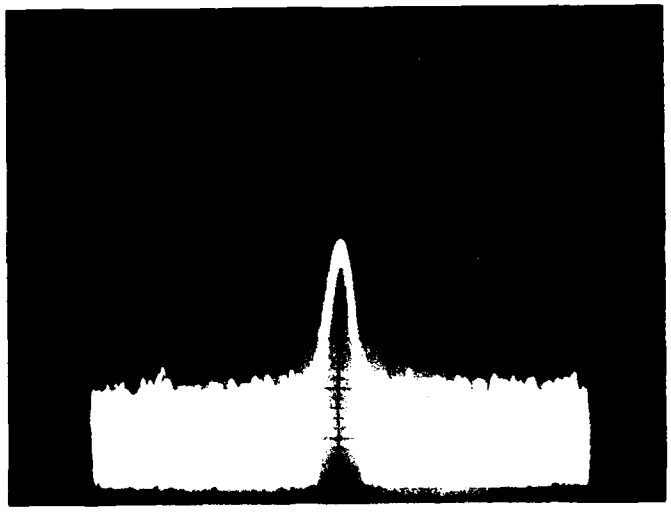

FIGURE A-10 MAXIMUM THIRD-HARMONIC SIGNAL FROM A PSEUDO-CRACK IN COPPER SAMPLE 10


DAT
FILM